Appendix A.5:

70 Langdons Rd – VsVp 57142

Table 1: Site Description for 70 Langdons Road (v_sv_p 57142).

Attribute	Yes/No			Description/Date	Symbol in Figure 1
	10-m Buffer	20-m Buffer	50-m Buffer		
Near a body of surface water or other free face features?	No	No	No	NA	NA
Lateral spreading observed during the CES?	No	No	No	Ground cracks indicating lateral spreading were not observed by the mapping team.[1]	NA
Nearby buildings or structures?	No	No	Yes	There are two structures in the 50-m buffer, one heavy in the SE quadrant and one light in the NW quadrant, covering a total of 2% of its area.	White Fill + Brown Outline
Sloping land?	No	No	No	NA	NA
Step changes in the ground surface?	No	No	No	NA	NA
Retaining walls?	No	No	No	NA	NA
Vegetation?	No	No	Yes	Trees and bushes are in the NW quadrant of the 20-m buffer covering 4% of its area and the NW, SW, and SE quadrants of the 50-m buffer covering 10% of its area.	White Fill + Green Outline
Anthropogenic changes to the site between the LiDAR surveys?	Yes	Yes	Yes	The empty grass lot became a construction site sometime at the end of 2014 and the beginning of 2015, altering the ground surface completely as earthwork was done and new structures were built.	NA (Please see Note 2)
Other important factors?	No	No	Yes	A busy two-way road runs through the SW quadrant and a small portion of the SE quadrant of the 50-m buffer, occupying 10% of its area. Two busy parking lots cover 20% of the 50-m buffer and are in its NW, SW, and SE quadrants. Slightly elevated property outline can be seen in the SE quadrant, affecting the 50-m buffer.	Property Outline: Purple Outline; Road and Parking Lots: White Fill + Gray Outline

Notes: Buffer is the area within a circle of a specified radius with VsVp investigations done at its center (172.604872, -43.492195); Oct 2015 LiDAR survey is excluded from the settlement analysis due to the anthropogenic changes.

[1] Canterbury Geotechnical Database. (2012). "Observed Ground Crack Locations", Map Layer CGD0400 - 23 July 2012, retrieved July 09, 2018 from https://canterburygeotechnicaldatabase.projectorbit.com/

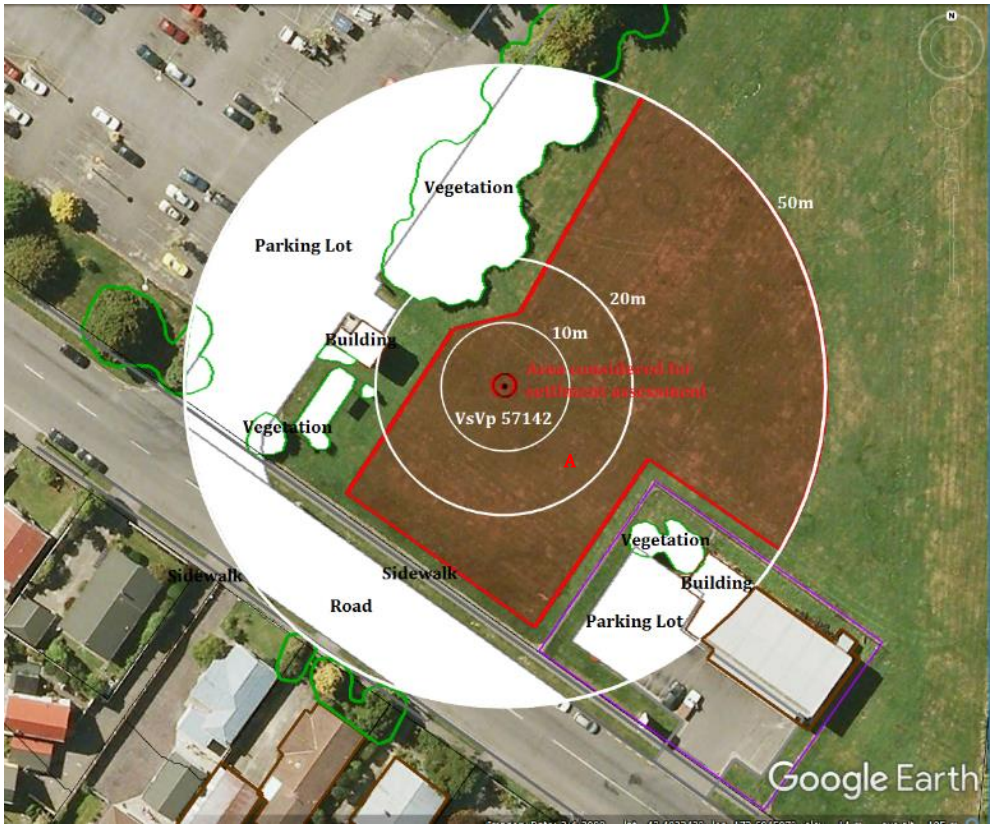

Figure 1: Site plan with areas where LiDAR survey data is considered.

Note 1: The area selected for settlement assessment (Patch A) is free of vegetation, structures, anthropogenic changes, and other important factors that have the potential to influence LiDAR measurements.

Table 2: LiDAR flight error adjustments, global adjustments for the difference between average LiDAR point elevations and benchmark survey elevations, and vertical tectonic movement adjustments.

	Adjustments (mm)		
Earthquake Event(s)	LiDAR Flight Error	Global Offset[2]	Tectonic Vertical Movement
Sep-10	NA	-3	0
Feb-11	NA	16	-40
Jun-11	0	38	-15
Dec-11	0	-65	0
CES	0	-14	-55
Any LiDAR survey affected by ejecta?			No

Notes: The negative sign indicates the subtraction from the ground surface subsidence, while the positive sign indicates the addition to the ground surface subsidence; NA = Not available.

[2] Russell, J., & van Ballegooy, S. (2015). *Canterbury Earthquake Sequence: Increased liquefaction vulnerability assessment methodology*. New Zealand: Tonkin & Taylor Ltd.

Table 3: LiDAR Measurement Error.

Surveys	Buffer	Area Averaged Difference Indicating Repeat Measurement Error (mm)	$\sigma^*_{\text{individual LiDAR points}}$ (mm)	%Reduction in σ due to Area Averaging of LiDAR Points
Post Feb 2011: Mar 2011 and May 2011	10-m	NA	59	NA
	20-m	NA		
	50-m	NA		
Post Dec 2011: Feb 2012 and Oct 2015	10-m	NA	70	NA
	20-m	NA		
	50-m	NA		

*Standard deviation.

Table 4: Ground surface subsidence adjustments due to LiDAR measurement error.

Earthquake Event(s)	$\sigma_{\text{pre-EQ LiDAR survey}}$ (mm)	$\sigma_{\text{post-EQ LiDAR survey}}$ (mm)	σ_{total} (mm)	Area Average Adjusted σ (mm) **
Sep-10	158	56	134	NA
Feb-11	56	59	59	NA
Jun-11	59	61	62	NA
Dec-11	61	70	87	NA
CES	158	70	124	NA

**Based on the highest %Reduction in Table 3.

Table 5: Raw liquefaction-related ground surface subsidence using original LiDAR points.

	Average Ground Surface Subsidence (mm)		
Earthquake Event(s)	10-m Buffer	20-m Buffer	50-m Buffer
Sep-10	NA	NA	NA
Feb-11	NA	NA	NA
Jun-11	-23	-20	-17
Dec-11	37	44	45
CES	108	114	129

Table 6: Corrected liquefaction-related ground surface subsidence using original LiDAR points with the calculated adjustments in Table 2.

	Average Calculated Ground Surface Subsidence (mm)		
Earthquake Event(s)	10-m Buffer	20-m Buffer	50-m Buffer
Sep-10	NA	NA	NA
Feb-11	NA	NA	NA
Jun-11	0 ± NA	3 ± NA	6 ± NA
Dec-11	-28 ± NA	-21 ± NA	-20 ± NA
CES	39 ± NA	45 ± NA	60 ± NA

Note: Plus/minus values are NA as per Table 4; Positive overall values indicate ground surface subsidence, while negative overall values indicate ground surface uplift.

Table 7: Corrected liquefaction-related ground surface subsidence using LiDAR DEMs.

	Estimated Ground Surface Subsidence (mm)								
	10-m Buffer			20-m Buffer			50-m Buffer		
Earthquake Event(s)	16^{th} %ile	50^{th} %ile	84^{th} %ile	16^{th} %ile	50^{th} %ile	84^{th} %ile	16^{th} %ile	50^{th} %ile	84^{th} %ile
Sep-10	NA	NA	NA	NA	NA	NA	NA	NA	NA
Feb-11	NA	NA	NA	NA	NA	NA	NA	NA	NA
Jun-11	50	50	50	50	50	50	50	50	50
Dec-11	50	50	50	50	50	50	50	50	50
CES	50	150	150	50	150	150	50	150	150

Note: These percentiles are not the exact statistical measures; they indicate the spatial variability of ground surface subsidence.

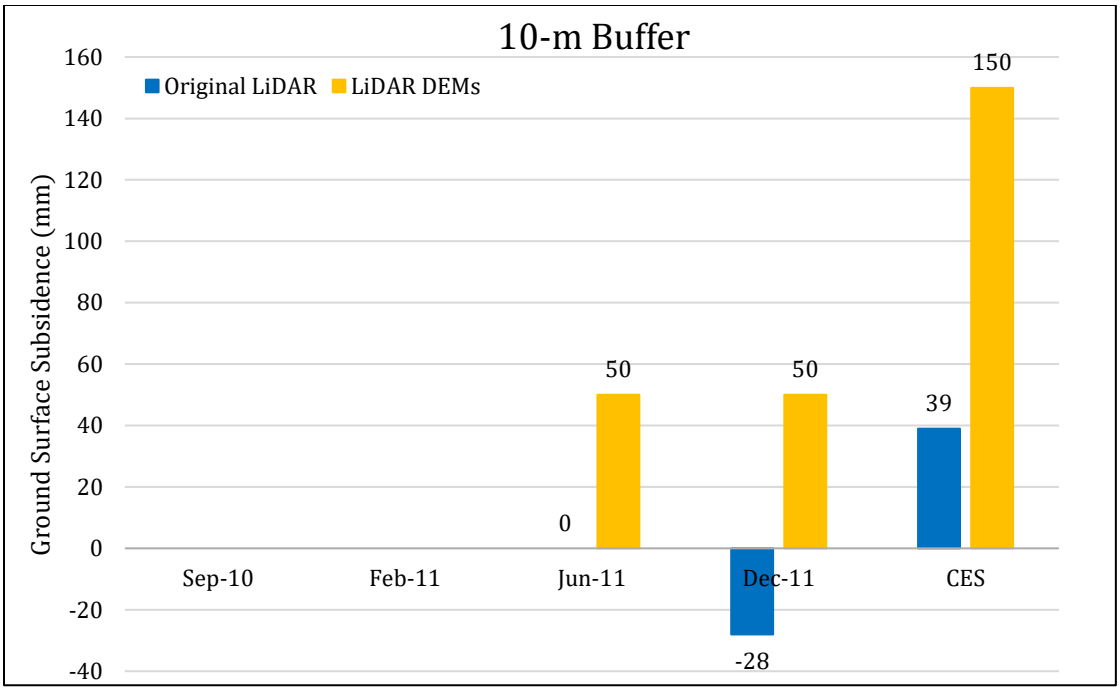

Figure 2: Comparison between ground surface subsidence determined from original LiDAR survey points and ground surface subsidence (50th %ile) estimated using LiDAR DEMs for the 10-m buffer.

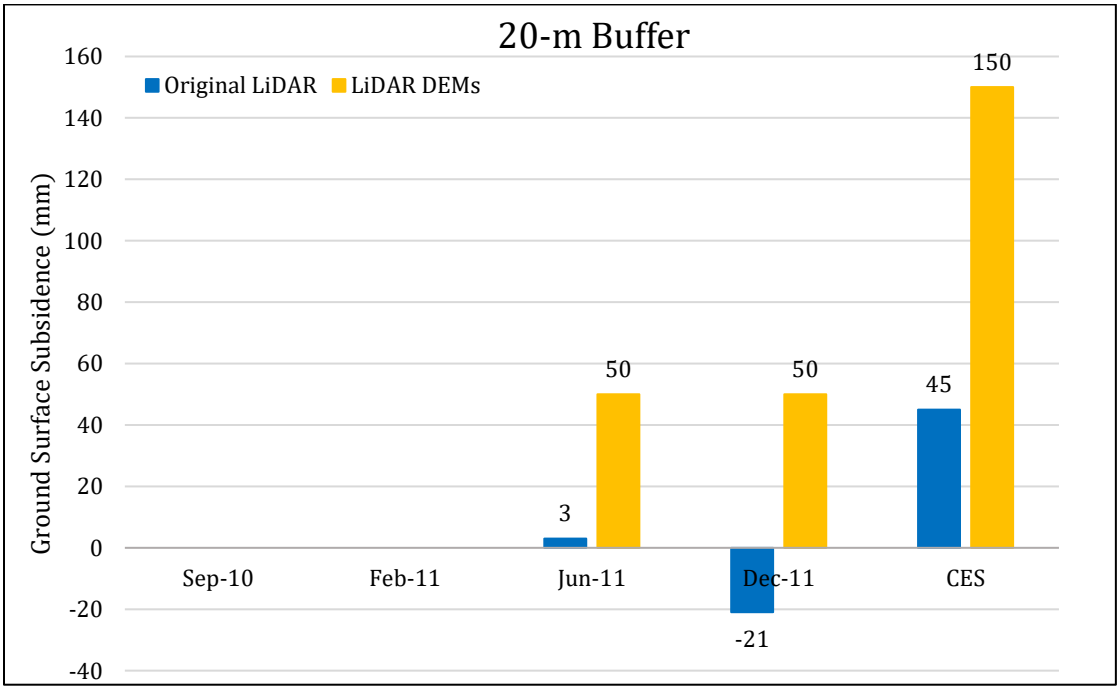

Figure 3: Comparison between ground surface subsidence determined from original LiDAR survey points and ground surface subsidence (50th %ile) estimated using LiDAR DEMs for the 20-m buffer.

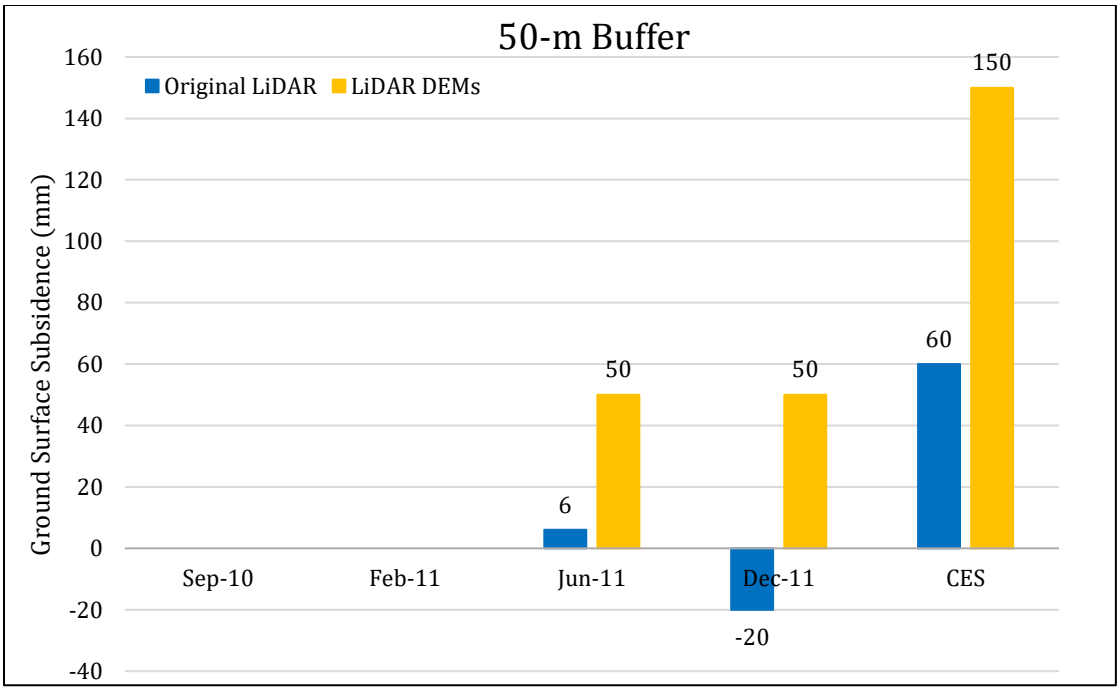

Figure 4: Comparison between ground surface subsidence determined from original LiDAR survey points and ground surface subsidence (50th %ile) estimated using LiDAR DEMs for the 50-m buffer.

Note 2: The ground surface subsidence values determined from original LiDAR survey points are fairly similar to the ground surface subsidence values estimated using LiDAR DEMs for Jun-11 Earthquake, Dec-11 Earthquake, and the CES.

Table 8a: Ejecta-Induced settlement for the top 20 m of the soil profile for the 10-m buffer for the 50th %ile PGA, P_L=50%, and C_{FC}=0.13 using BI-2014, ZRB-2002, and I_C cutoff of 2.6.

Earthquake Event(s)	M_W	PGA (g)	Depth to Groundwater (m)	S_T(mm)	S_{V1D} (mm)	$S_{E,L}$ (mm)
Sep-10	7.1	0.21	1.5	NA	75±20	NA
Feb-11	6.2	0.23	1.5	NA	70±50	NA
Jun-11	6.2	0.13	1.5	0±NA	4±25	-4±NA
Dec-11	6.1	0.15	1.5	-28±NA	11±50	-39±NA

Notes: S_T = Total settlement (Table 6); S_{V1D} = Average vertical settlement due to volumetric compression using Boulanger and Idriss (2014) (BI-2014) and Zhang et al. (2002) (ZRB-2002) procedures and de Greef and Lengkeek (2018) thin-layer correction; $S_{E,L}$ = Ejecta-induced settlement as the difference between the LiDAR-based S_T and S_{V1D}; NA = Not available; NE = Not evaluated.

Table 8b: Ejecta-Induced settlement for the top 20 m of the soil profile for the 20-m buffer for the 50th %ile PGA, P_L=50%, and C_{FC}=0.13 using BI-2014, ZRB-2002, and I_C cutoff of 2.6.

Earthquake Event(s)	M_W	PGA (g)	Depth to Groundwater (m)	S_T(mm)	S_{V1D} (mm)	$S_{E,L}$ (mm)
Sep-10	7.1	0.21	1.5	NA	75±20	NA
Feb-11	6.2	0.23	1.5	NA	70±50	NA
Jun-11	6.2	0.13	1.5	3±NA	4±25	-1±NA
Dec-11	6.1	0.15	1.5	-21±NA	11±50	-32±NA

Notes: S_T = Total settlement (Table 6); S_{V1D} = Average vertical settlement due to volumetric compression using Boulanger and Idriss (2014) (BI-2014) and Zhang et al. (2002) (ZRB-2002) procedures and de Greef and Lengkeek (2018) thin-layer correction; $S_{E,L}$ = Ejecta-induced settlement as the difference between the LiDAR-based S_T and S_{V1D}; NA = Not available.

Table 8c: Ejecta-Induced settlement for the top 20 m of the soil profile for the 50-m buffer for the 50th %ile PGA, P_L=50%, and C_{FC}=0.13 using BI-2014, ZRB-2002, and I_C cutoff of 2.6.

Earthquake Event(s)	M_W	PGA (g)	Depth to Groundwater (m)	S_T(mm)	S_{V1D} (mm)	$S_{E,L}$ (mm)
Sep-10	7.1	0.21	1.5	NA	92±20	NA
Feb-11	6.2	0.23	1.5	NA	82±50	NA
Jun-11	6.2	0.13	1.5	6±NA	4±25	2±NA
Dec-11	6.1	0.15	1.5	-20±NA	12±50	-32±NA

Notes: S_T = Total settlement (Table 6); S_{V1D} = Average vertical settlement due to volumetric compression using Boulanger and Idriss (2014) (BI-2014) and Zhang et al. (2002) (ZRB-2002) procedures and de Greef and Lengkeek (2018) thin-layer correction; $S_{E,L}$ = Ejecta-induced settlement as the difference between the LiDAR-based S_T and S_{V1D}; NA = Not available.

Note 3: The uncertainty for volumetric settlement was derived based on the sensitivity of volumetric settlement to PGA, C_{FC}, and P_L for each earthquake event for VsVp 57203 *Shirley Intermediate School* and CC LIQ 1 – CPT 5586 – *Vivian St* sites. Taking the 50th percentile as the baseline case, the minimum and maximum values corresponding to the difference between the 25th percentile and the 50th percentile and the 75th percentile and the 50th percentile were determined. The arithmetic mean of the range of the minimum and maximum difference was evaluated for each patch at the two sites. The maximum arithmetic mean for each earthquake event was rounded to the nearest five and used as the uncertainty value. Accordingly, the 1-D volumetric settlement uncertainties of ±20, ±50, ±25, and ±50 mm for the Sep-10, Feb-11, Jun-11, and Dec-11 earthquake events, respectively, were used for all sites in this study.

Table 9a: Coverage area and height of ejecta estimates for the 10-m buffer using photographs.

Earthquake Event	$A_{E,thick}$ (m^2)	$H_{E,thick}$ (mm)	$A_{E,thin}$ (m^2)	$H_{E,thin}$ (mm)	A_T (m^2)
Sep-10	0	0	0	0	314
Feb-11	0	0	0	0	314
Jun-11	0	0	0	0	314
Dec-11*	0	0	0	0	314

Notes: $A_{E,thick/thin}$ =Coverage area of thick/thin ejecta layers; $H_{E,thick/thin}$ = Lower-upper estimate of height of thick/thin ejecta layers; A_T= Total assessment area of a buffer being considered; Thin and thick layers correspond to light gray and dark gray colors of ejecta observed in aerial photographs; NA = Not applicable available as no aerial and/or ground photographs were acquired for the site; * indicates uncertainty due to the lack of physical evidence.

Table 9b: Coverage area and height of ejecta estimates for the 20-m buffer using photographs.

Earthquake Event	$A_{E,thick}$ (m^2)	$H_{E,thick}$ (mm)	$A_{E,thin}$ (m^2)	$H_{E,thin}$ (mm)	A_T (m^2)
Sep-10	0	0	0	0	982
Feb-11	0	0	0	0	982
Jun-11	0	0	0	0	982
Dec-11*	0	0	0	0	982

Notes: $A_{E,thick/thin}$ =Coverage area of thick/thin ejecta layers; $H_{E,thick/thin}$ = Lower-upper estimate of height of thick/thin ejecta layers; A_T= Total assessment area of a buffer being considered; Thin and thick layers correspond to light gray and dark gray colors of ejecta observed in aerial photographs; NA = Not available as no aerial and/or ground photographs were acquired for the site; * indicates uncertainty due to the lack of physical evidence.

Table 9c: Coverage area and height of ejecta estimates for the 50-m buffer using photographs.

Earthquake Event	$A_{E,thick}$ (m^2)	$H_{E,thick}$ (m)	$A_{E,thin}$ (m^2)	$H_{E,thin}$ (m)	A_T (m^2)
Sep-10	0	0	0	0	3218
Feb-11	0	0	0	0	3218
Jun-11	0	0	0	0	3218
Dec-11*	0	0	0	0	3218

Notes: $A_{E,thick/thin}$ =Coverage area of thick/thin ejecta layers; $H_{E,thick/thin}$ = Lower-upper estimate of height of thick/thin ejecta layers; A_T= Total assessment area of a buffer being considered; Thin and thick layers correspond to light gray and dark gray colors of ejecta observed in aerial photographs; NA = Not available as no aerial and/or ground photographs were acquired for the site; * indicates uncertainty due to the lack of physical evidence.

Note 4: The values in Table 9 are based on aerial photographs (Figures 49, 50, and 52) and liquefaction interpreted from aerial photographs and observations made by inspection teams (Figures 51, 53, and 54). The ejecta-induced settlement using photographs and engineering judgment, $S_{E,P}$, is estimated as

$$S_{E,P} = \frac{\sum_{i=1}^{n} A_{E,thick,i} * H_{E,thick,i} + \sum_{j=1}^{m} A_{E,thin,j} * H_{E,thin,j}}{A_T}$$

where $A_{E,thick,i}$ and $H_{E,thick,i}$ are the area and the height of a thick ejecta layer, respectively, $A_{E,thin,j}$ and $H_{E,thin,j}$ are the area and the height of a thin ejecta layer, respectively, and A_T is the total assessment area for a buffer being considered (Figure 1). The $A_{E,thick,i}$ and $A_{E,thin,i}$ are contained within the buffer.

Table 10: Ejecta-induced settlement estimates based on photographs.

Earthquake Event	10-m buffer		20-m buffer		50-m buffer	
	$S_{E,P,lower}$ (mm)	$S_{E,P,upper}$ (mm)	$S_{E,P,lower}$ (mm)	$S_{E,P,upper}$ (mm)	$S_{E,P,lower}$ (mm)	$S_{E,P,upper}$ (mm)
Sep-10	0	0	0	0	0	0
Feb-11	0	0	0	0	0	0
Jun-11	0	0	0	0	0	0
Dec-11*	0	0	0	0	0	0

Notes: $S_{E,P,lower}$ and $S_{E,P,upper}$ correspond to lower and upper estimates of $S_{E,P}$, respectively; * indicates uncertainty due to the lack of physical evidence.

Table 11: Best final estimates of ejecta-induced settlement.

Earthquake Event	10-m buffer			20-m buffer			50-m buffer		
	$S_{E,L}$ (mm)	$S_{E,P}$ (mm)	$S_{E,final}$ (mm)	$S_{E,L}$ (mm)	$S_{E,P}$ (mm)	$S_{E,final}$ (mm)	$S_{E,L}$ (mm)	$S_{E,P}$ (mm)	$S_{E,final}$ (mm)
Sep-10	NA	0	0	NA	0	0	NA	0	0
Feb-11	NA	0	0	NA	0	0	NA	0	0
Jun-11	-4±NA	0	0	-1±NA	0	0	2±NA	0	0
Dec-11	-39±NA	0*	0*	-32±NA	0*	0*	-32±NA	0*	0*

Notes: $S_{E,L}$ = Ejecta-induced settlement based on LiDAR data reported in Table 8; $S_{E,P}$ = Median ejecta-induced settlement for the range of values reported in Table 10; $S_{E,final}$ = Best final estimate of ejecta-induced settlement rounded to the nearest 5; Final plus/minus values are also rounded to the nearest 5; * indicates uncertainty due to the lack of physical evidence.

Note 5: $S_{E,final}$ for the Sep-10, Feb-11, and Jun-11 earthquakes is based solely on $S_{E,P}$. The 70 Langdons Rd site is in the zone of slight to moderate LPI overprediction of liquefaction severity for the Sep-10 earthquake (Maurer et al. 2014[3]). The LPI prediction of liquefaction severity for the Feb-11 earthquake is accurate (Maurer et al. 2014). There is no high-resolution aerial or satellite photograph

[3] Maurer, B. W., Green, R. A., Cubrinovski, M., & Bradley, B. A. (2014). Evaluation of the Liquefaction Potential Index for Assessing Liquefaction Hazard in Christchurch, New Zealand. *Journal of Geotechnical and Geoenvironmental Engineering*, 140(7), 04014032-1-11. doi:10.1061/(asce)gt.1943-5606.0001117

or ground photograph for the site for the Jun-11 earthquake, only on-foot rapid inspection of Langdons Rd for liquefaction manifestation at the ground surface following the earthquake. For the Dec-11 earthquake, Figure 54 shows "liquefaction interpreted from aerial photography" as minor even though there is no actual aerial photograph for the site to support the claim. There is also no LDAT property inspection report or ground photographs for the Dec-11 earthquake. However, the seismic demand on the soil profile during the Dec-11 event is not significantly different than that during the Jun-11 event or worse than those during the Sep-10 and Feb-11 events; thus, it is reasonable to assume that the Dec-11 did not cause ejecta at the site.

Summary: The best estimate of the ejecta-induced free-field ground settlement at the 70 Langdons Road site for the SEP 2010, FEB 2011, JUN 2011, and DEC 2011 earthquake is 0 mm, 0 mm, 0 mm, and 0 mm, respectively.

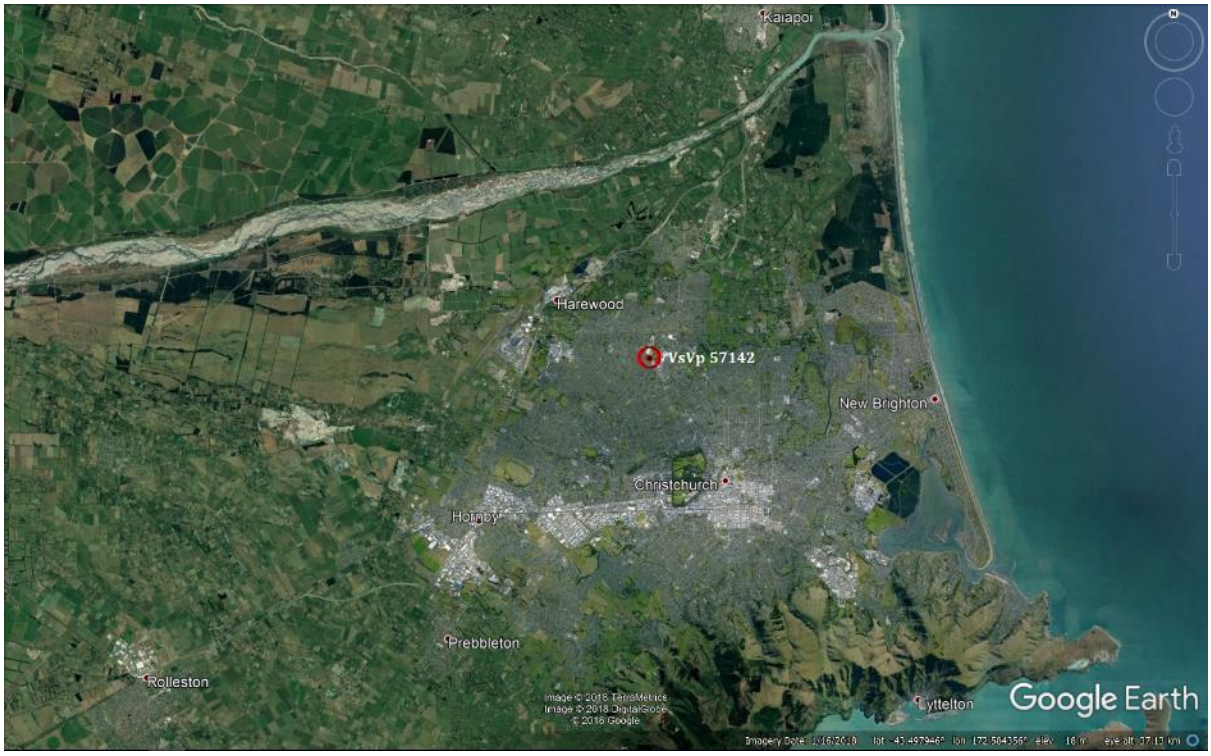

Figure 5: Location of the site.

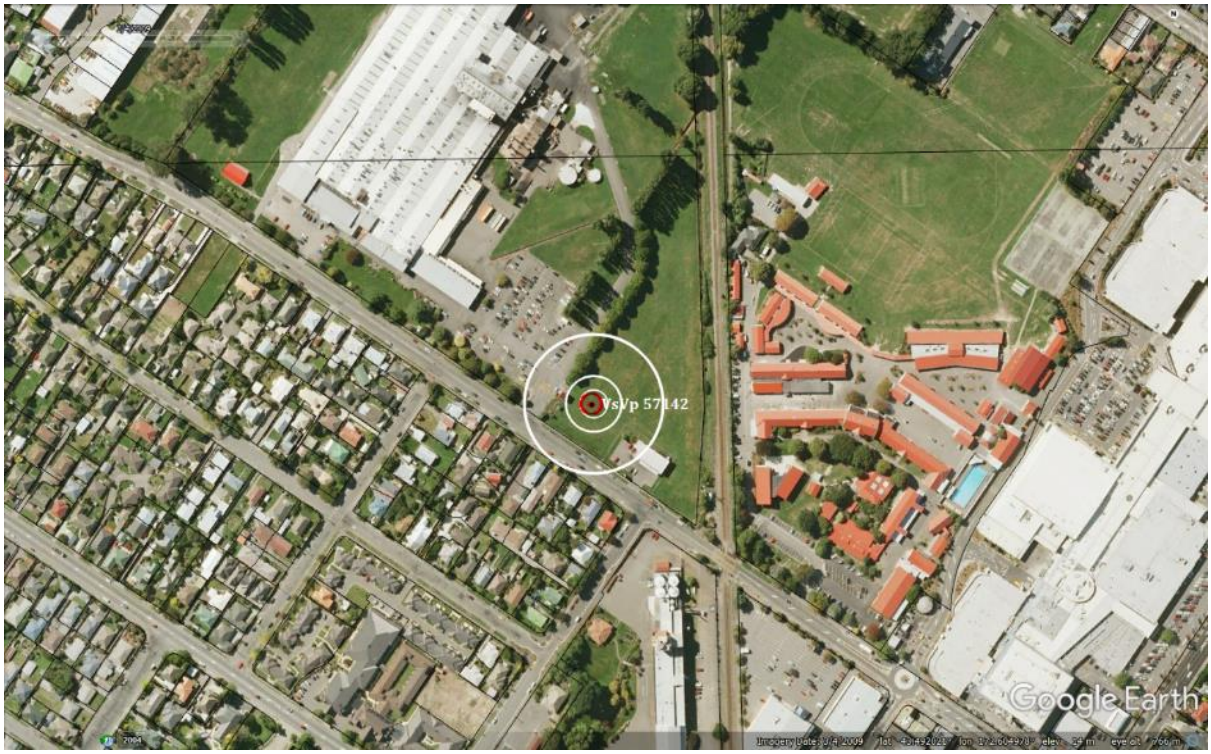

Figure 6: Position of the site relative to nearby buildings, vegetation, and other important features.

Figure 7: Street view of the flat land.

Figure 8: Aerial photograph of the site taken in Apr 2004.

Figure 9. Aerial photograph of the site taken on Sep 4, 2010.

Figure 10. Aerial photograph of the site taken on Sep 6, 2010.

Figure 11: Aerial photograph of the site taken on Feb 27, 2011.

Figure 12: Aerial photograph of the site taken in Apr 2012.

Figure 13: Aerial photograph of the site taken in Jan 2015.

Figure 14: Aerial photograph of the site taken in Nov 2015.

Figure 15. EQC Aerial Photograph of the site taken on Sep 5, 2010 is not available.

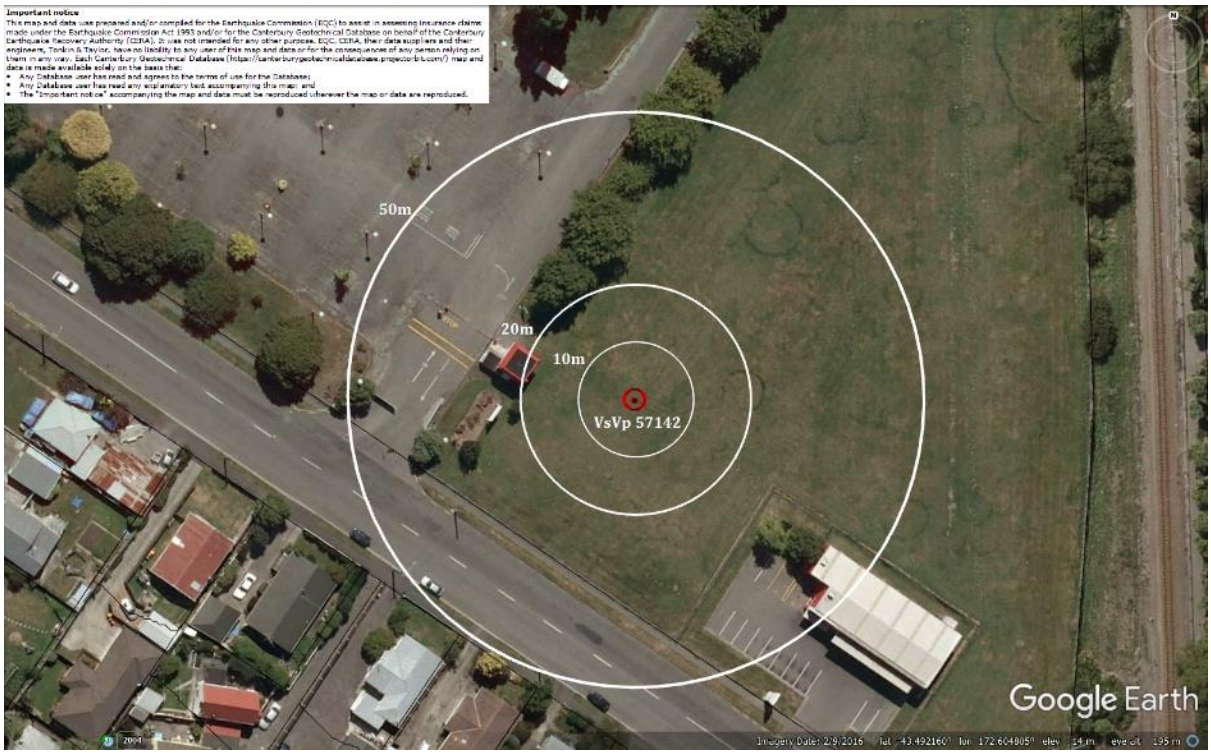

Figure 16: EQC Aerial Photograph of the site taken on Feb 24, 2011.

Figure 17: EQC Aerial Photograph of the site taken on June 16, 2011 is not available (neither is the one from June 14-15, 2011).

Figure 18: EQC Aerial Photograph of the site taken on Dec 24, 2011 is not available.

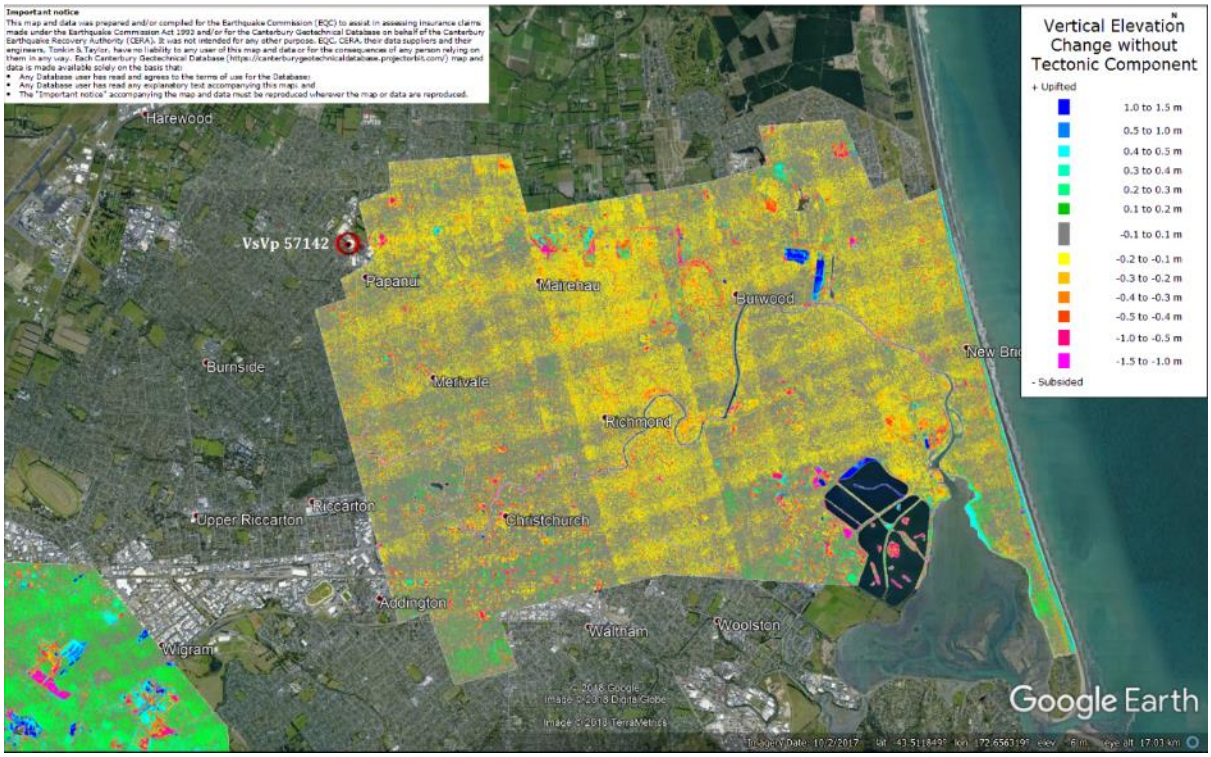

Figure 19: Vertical Ground Movements (Surface – Tectonic) for Sep 2010 Earthquake for the site are not available.

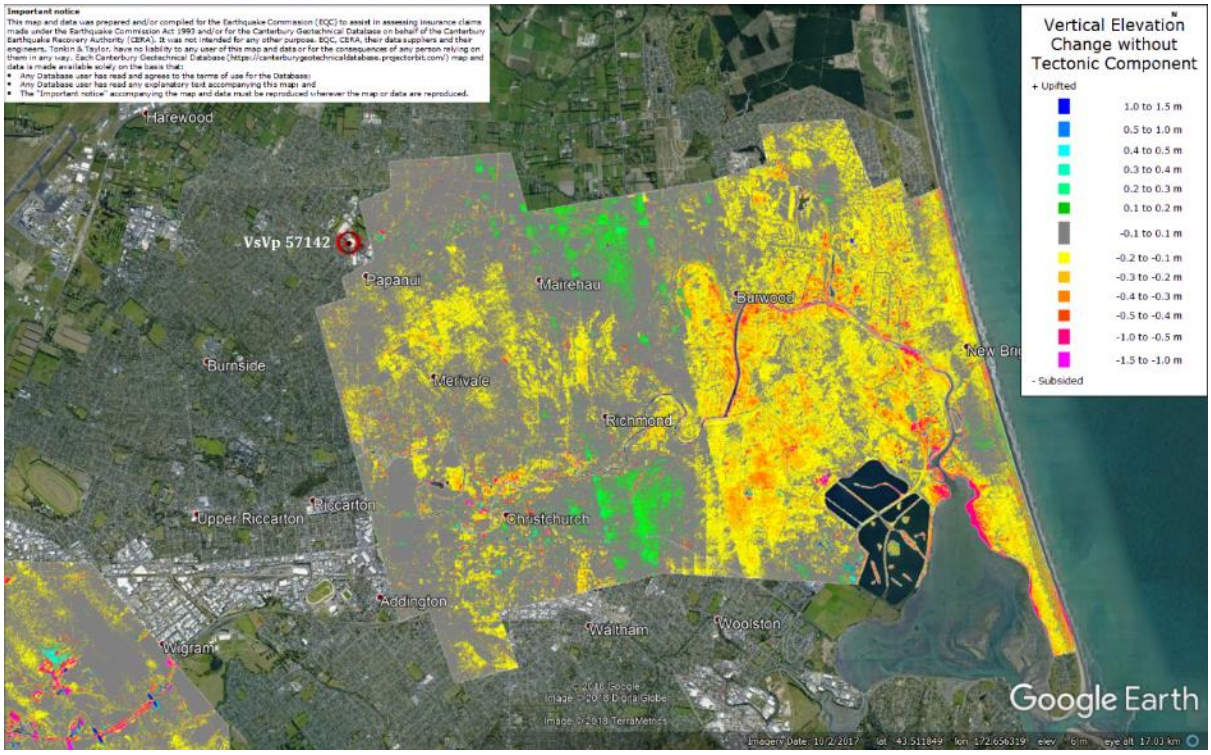

Figure 20: Vertical Ground Movements (Surface – Tectonic) for Feb 2011 Earthquake for the site are not available.

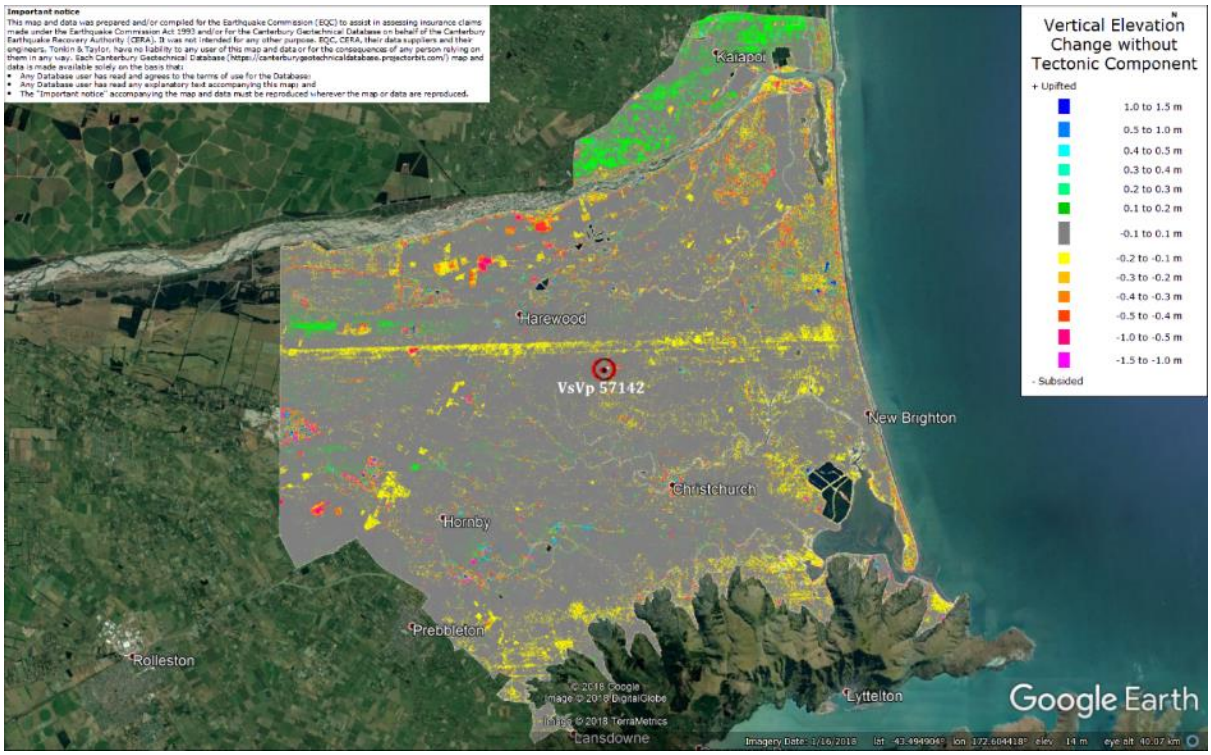

Figure 21: Vertical Ground Movements (Surface – Tectonic) for June 2011 Earthquake – the site is not in the apparent zone of overestimated or underestimated ground surface subsidence.

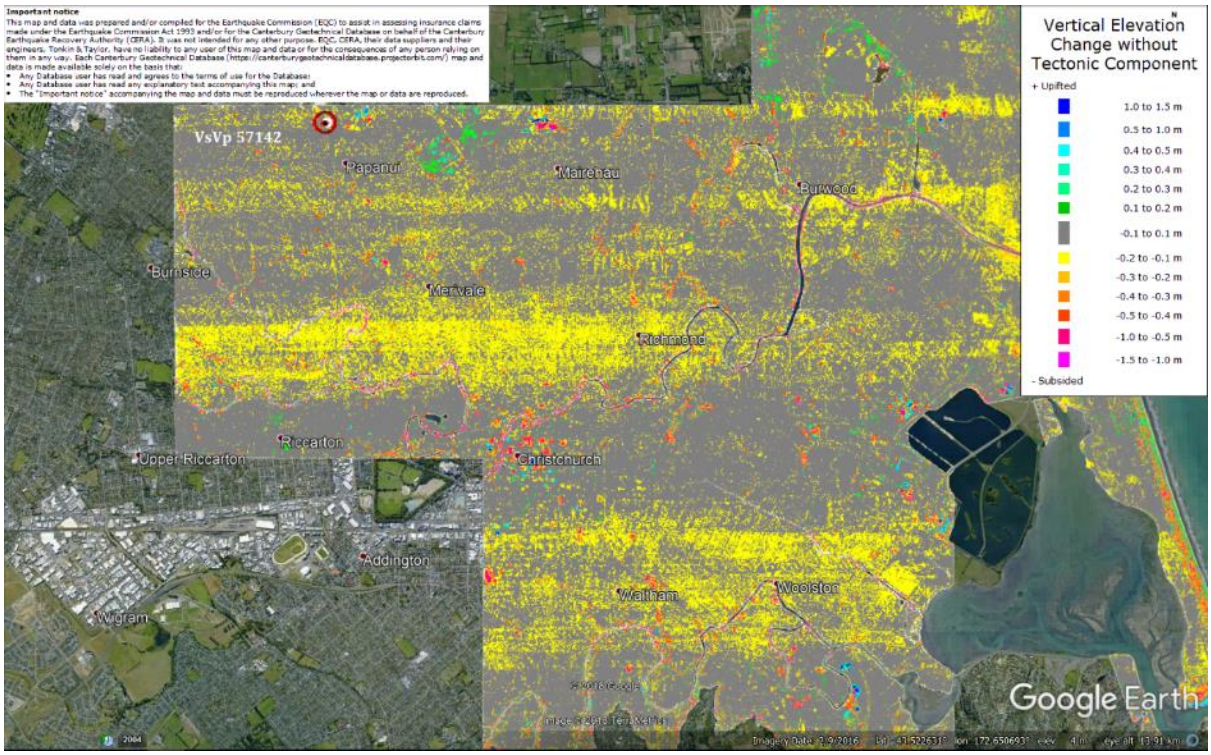

Figure 22: Vertical Ground Movements (Surface – Tectonic) for Dec 2011 Earthquake – the site is not in the apparent zone of overestimated or underestimated ground surface subsidence.

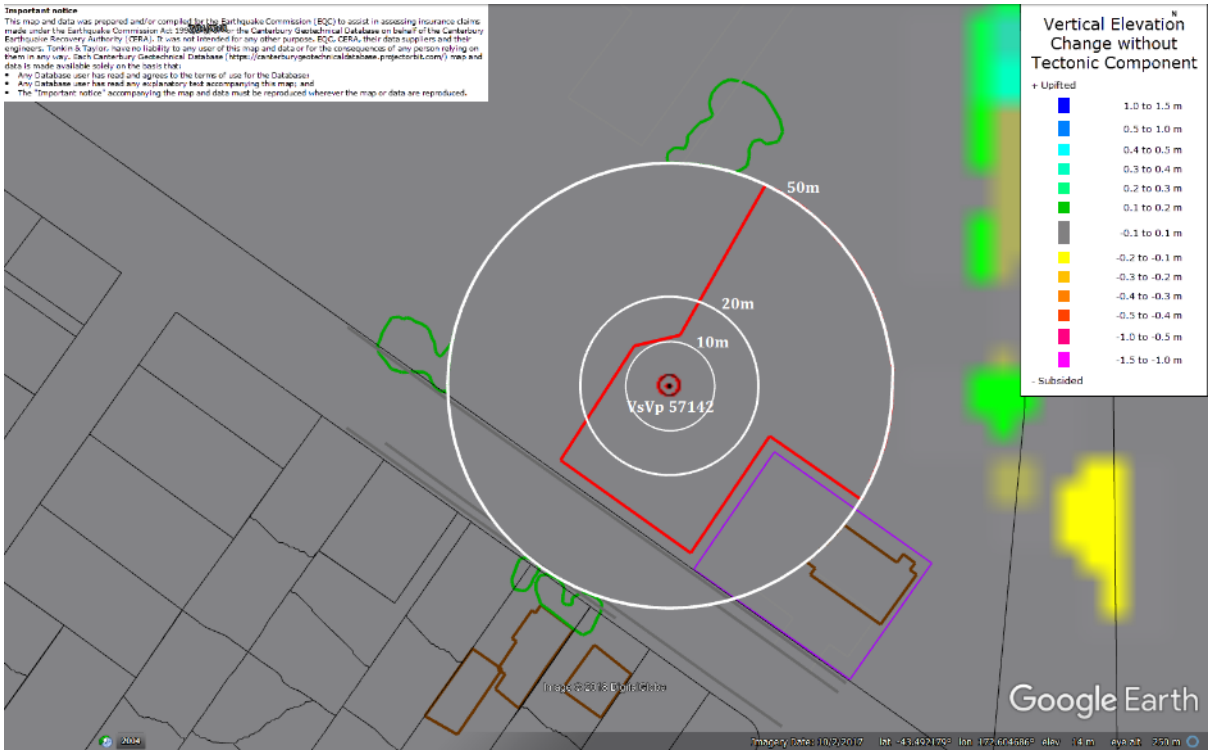

Figure 23: LiDAR DEM-based ground surface subsidence without tectonic component for Jun 2011 Earthquake.

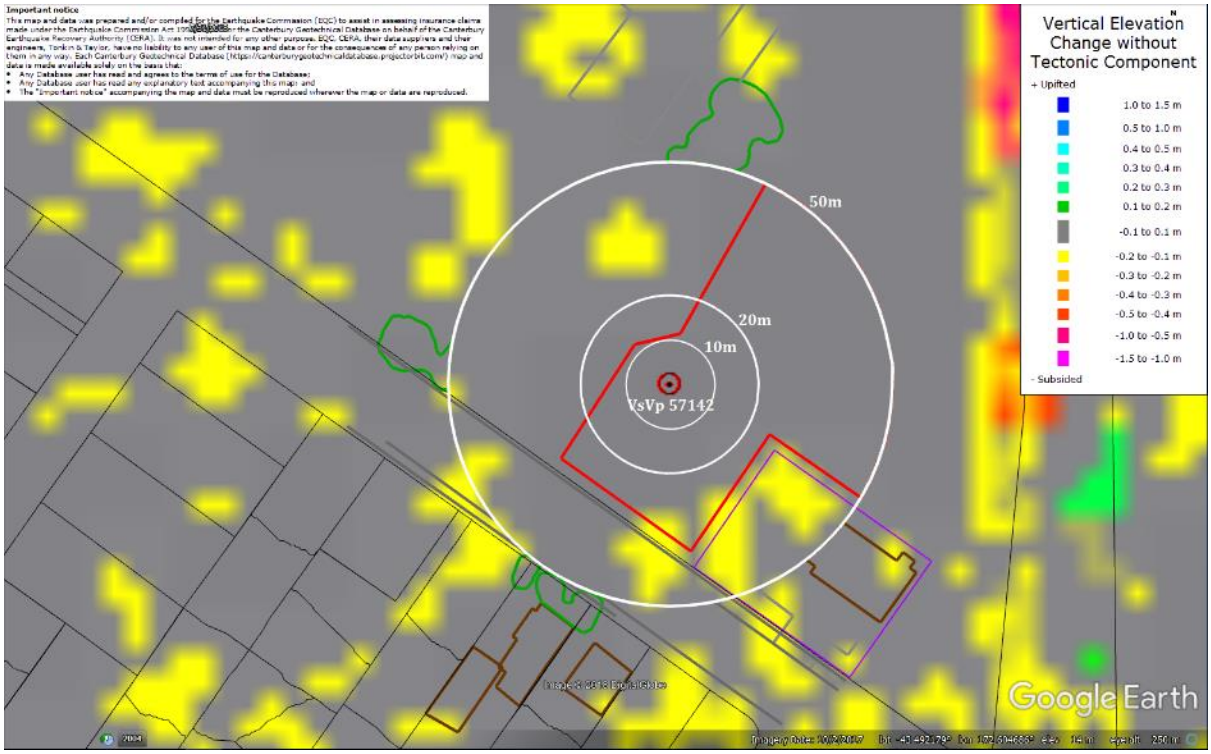

Figure 24: LiDAR DEM-based ground surface subsidence without tectonic component for Dec 2011 Earthquake.

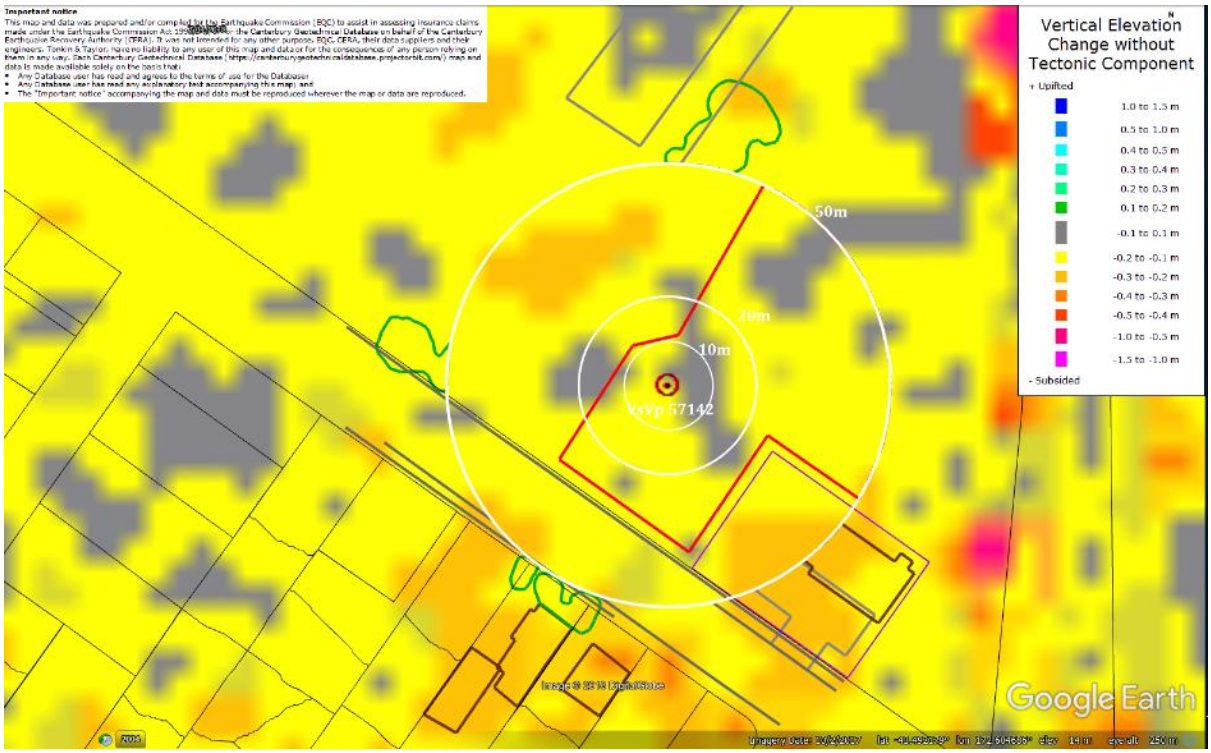

Figure 25: LiDAR DEM-based ground surface subsidence without tectonic component for CES.

Note 6: LiDAR DEM-based ground surface subsidence without tectonic component is not available for Sep 2010 and Feb 2011 earthquake events. The available LiDAR surveys for this site are dated to Jun 2003, May 2011, Sep 2011, and Feb 2012.

Figure 26: Absence of ground cracks indicating no lateral spreading for Canterbury Earthquake Sequence.

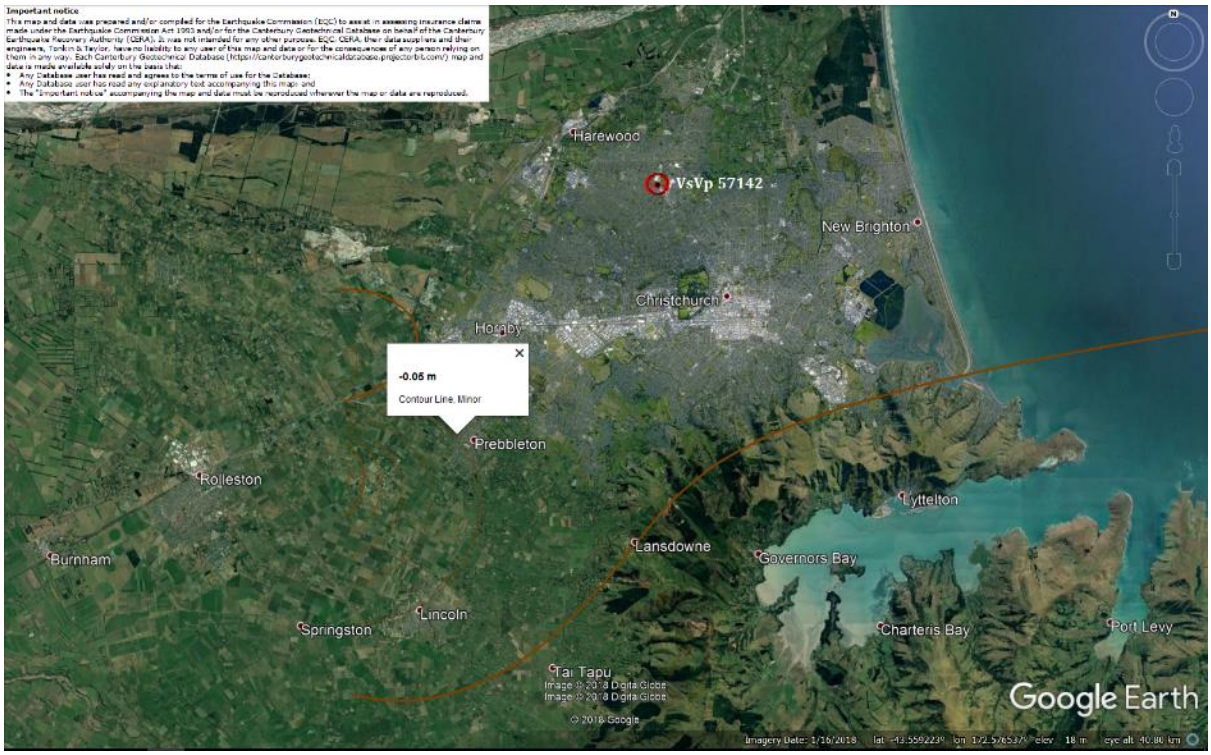

Figure 27: Vertical tectonic movements for Sep 2010 Earthquake.

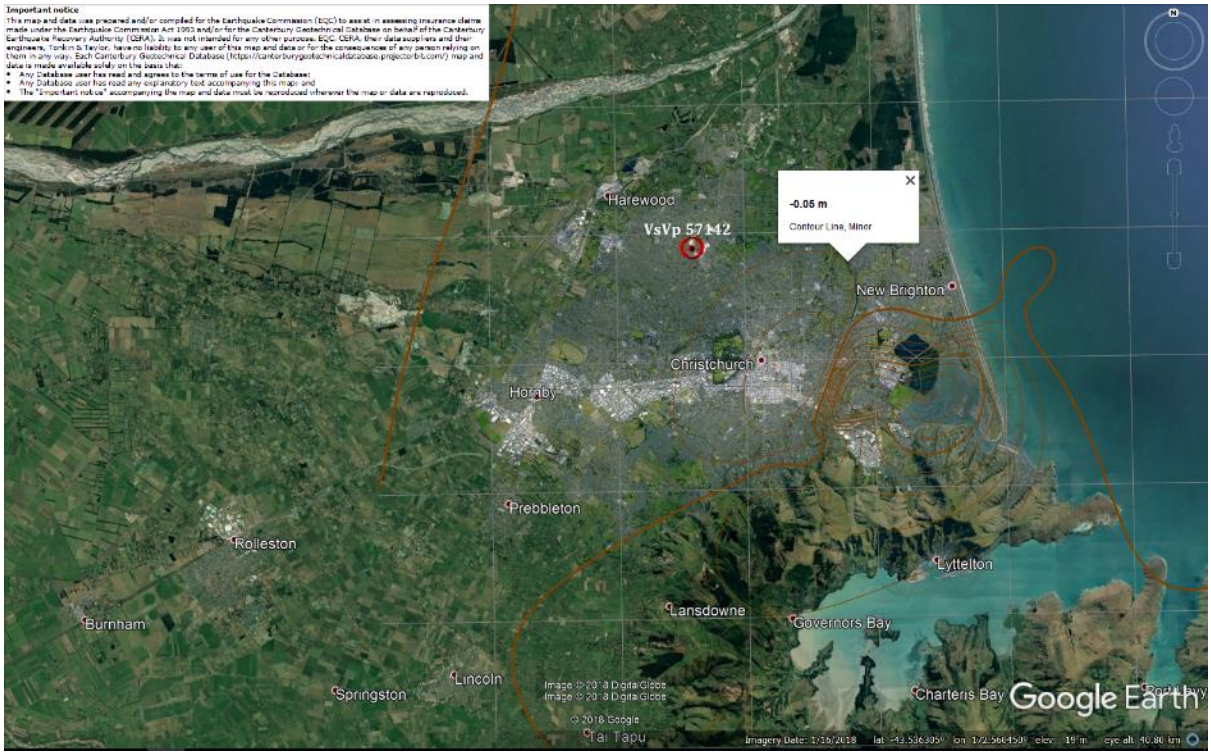

Figure 28: Vertical tectonic movements for Feb 2011 Earthquake.

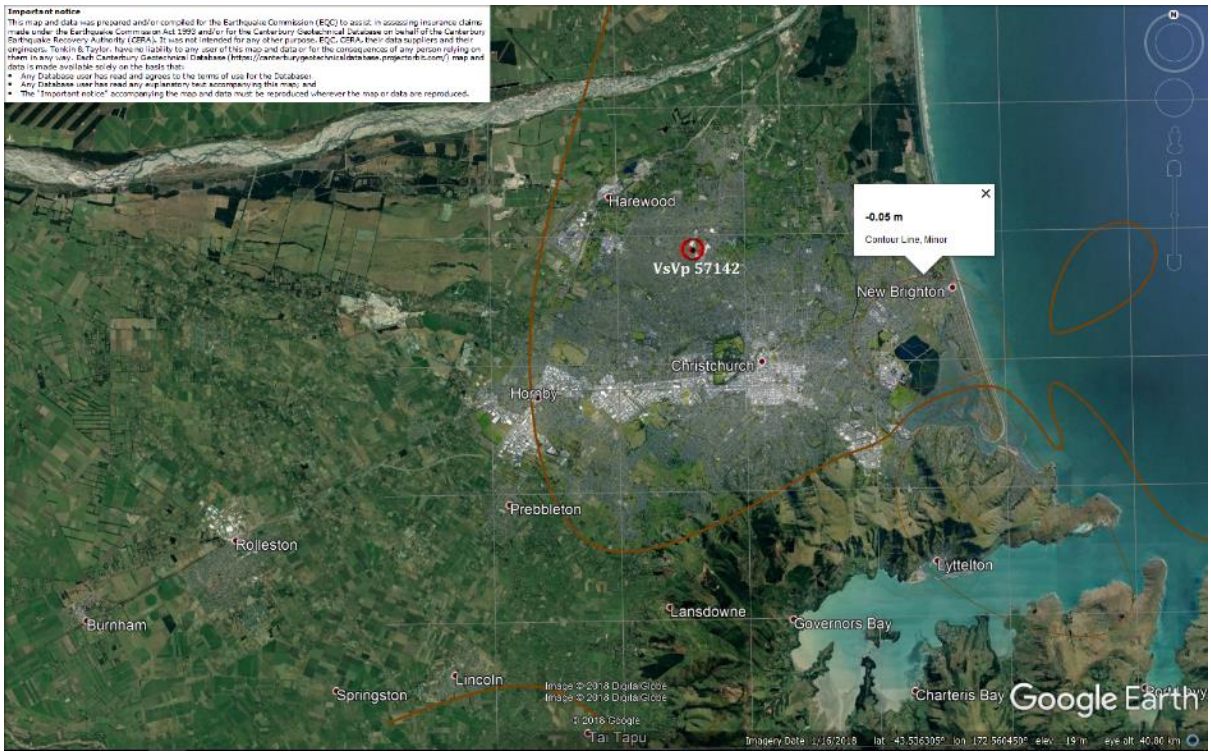

Figure 29: Vertical tectonic movements for June 2011 Earthquake.

Figure 30: Vertical tectonic movements for Dec 2011 Earthquake.

Figure 31: Vertical tectonic movements for Canterbury Earthquake Sequence.

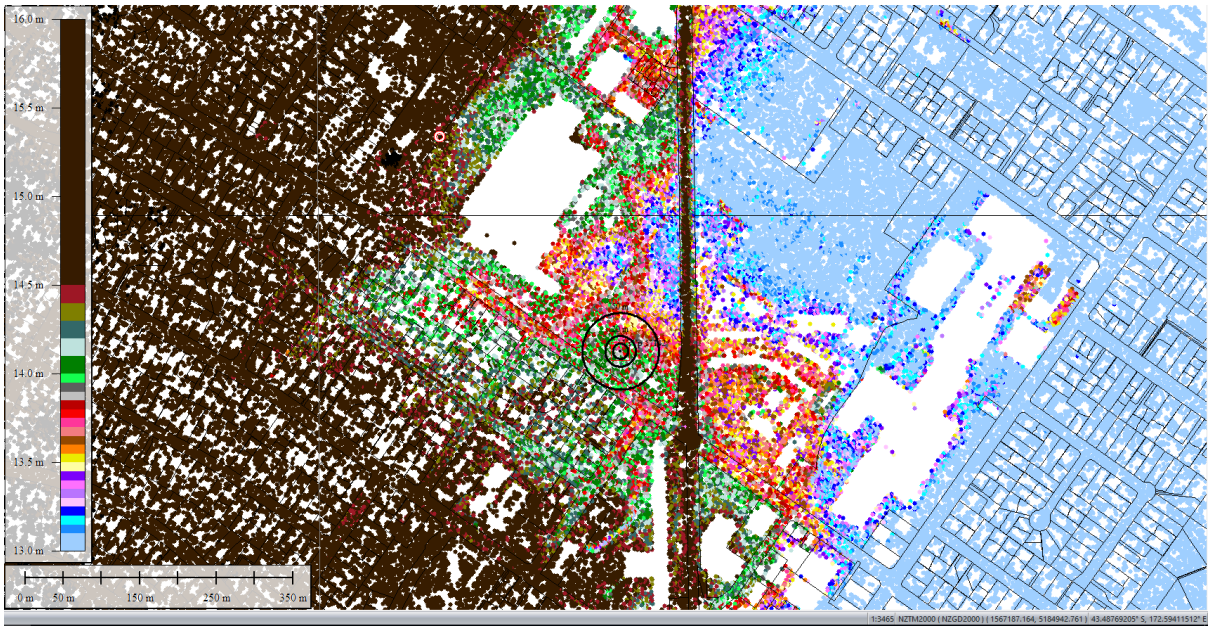

Figure 32: Jul 2003 LiDAR survey.

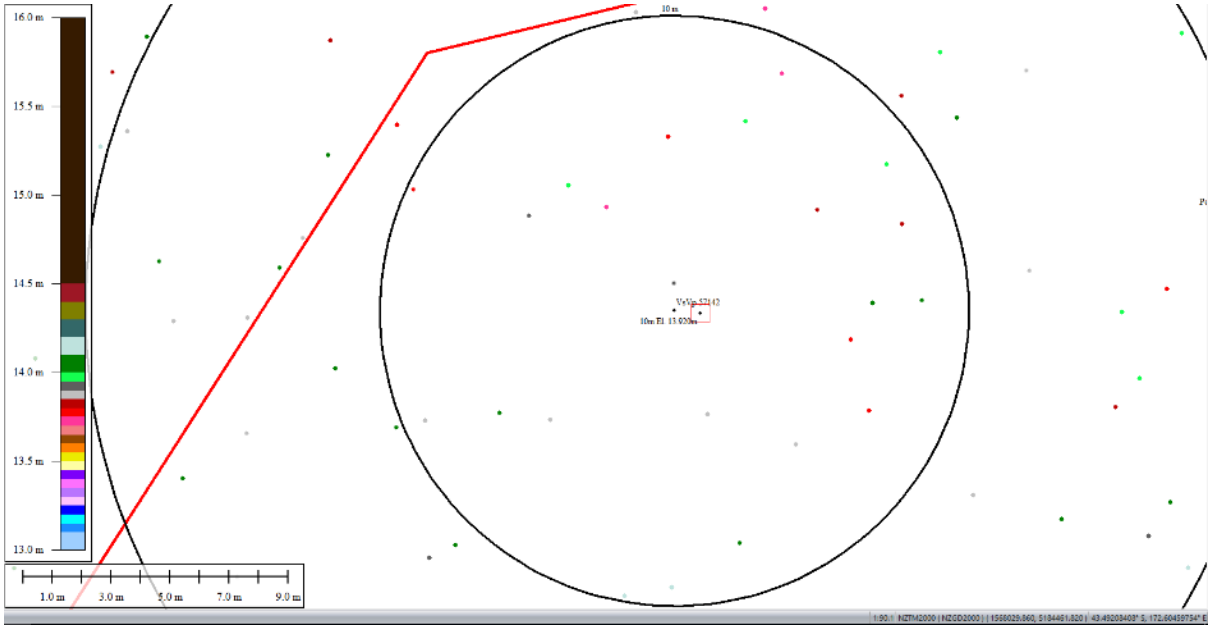

Figure 33: Ground surface elevation averaged over 10-m buffer for Jul 2003 LiDAR survey.

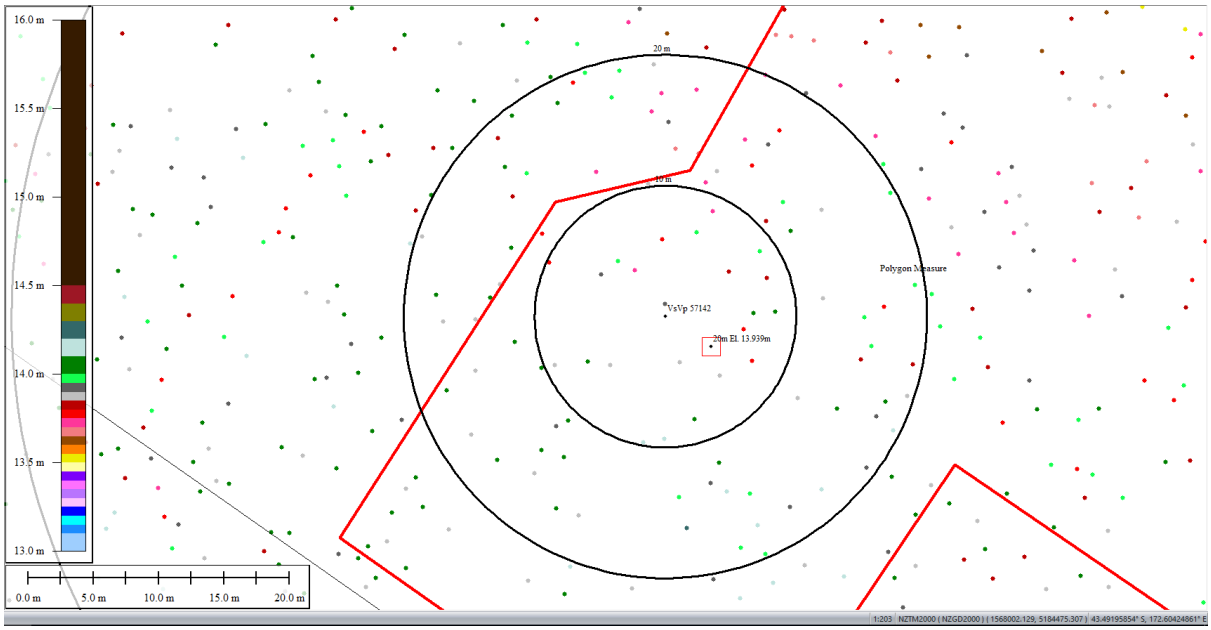

Figure 34: Ground surface elevation averaged over 20-m buffer for Jul 2003 LiDAR survey.

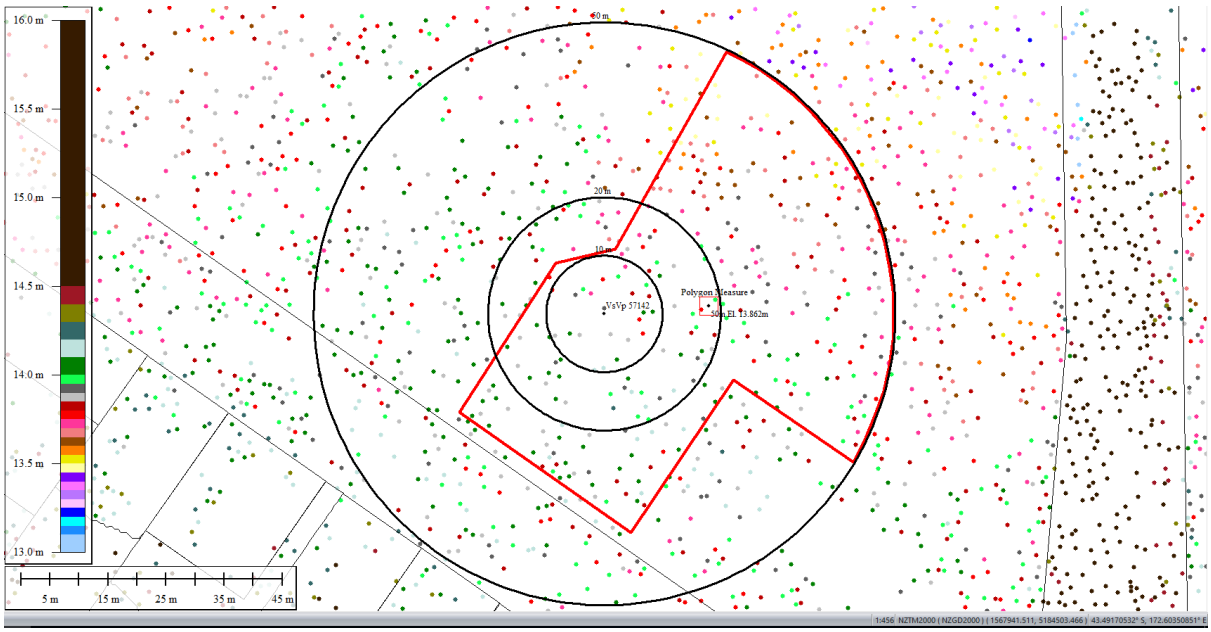

Figure 35: Ground surface elevation averaged over 50-m buffer for Jul 2003 LiDAR survey.

Note 7: Sep 2010 and Mar 2011 LiDAR surveys are not available.

Figure 36: May 2011 LiDAR survey.

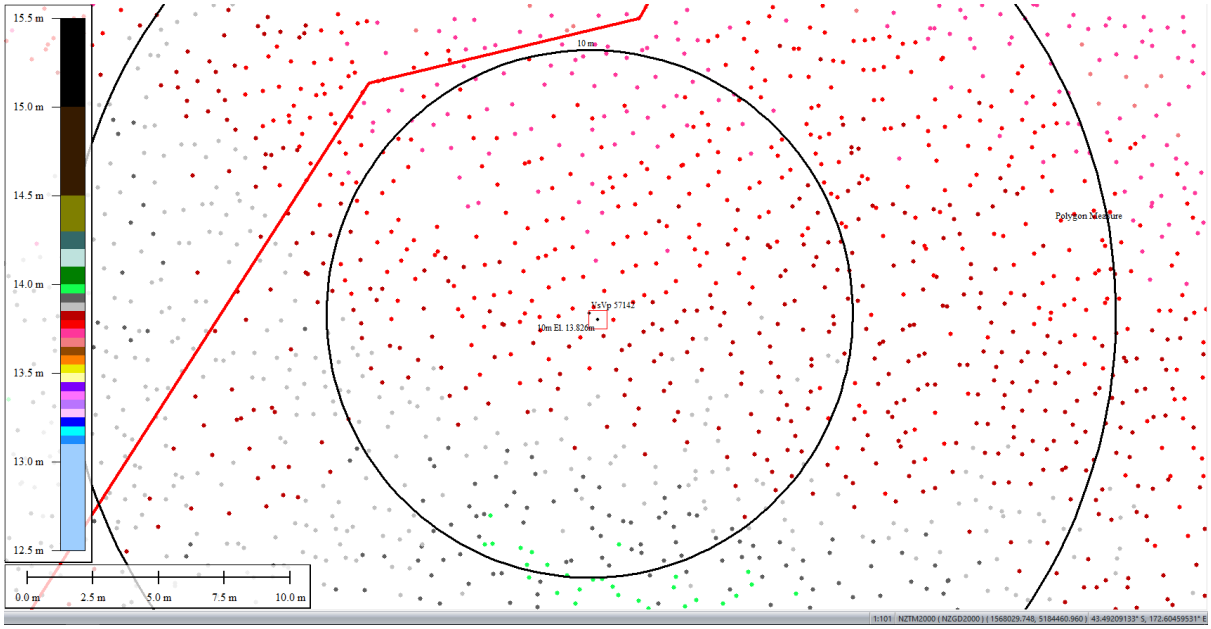

Figure 37: Ground surface elevation averaged over 10-m buffer for May 2011 LiDAR survey.

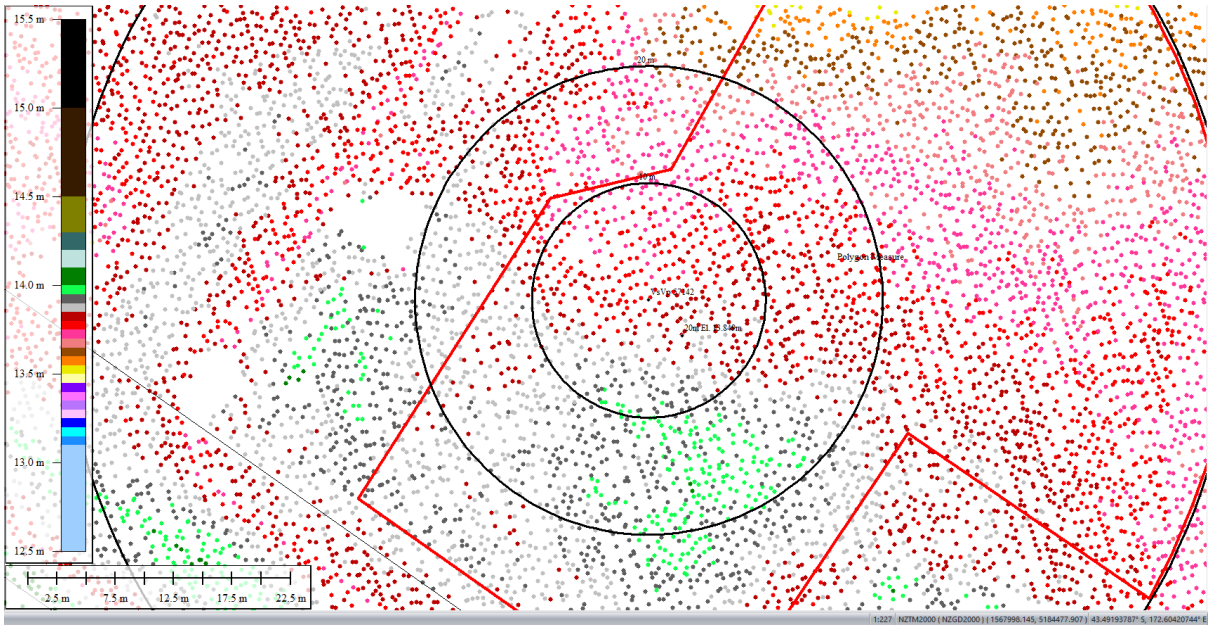

Figure 38: Ground surface elevation averaged over 20-m buffer for May 2011 LiDAR survey.

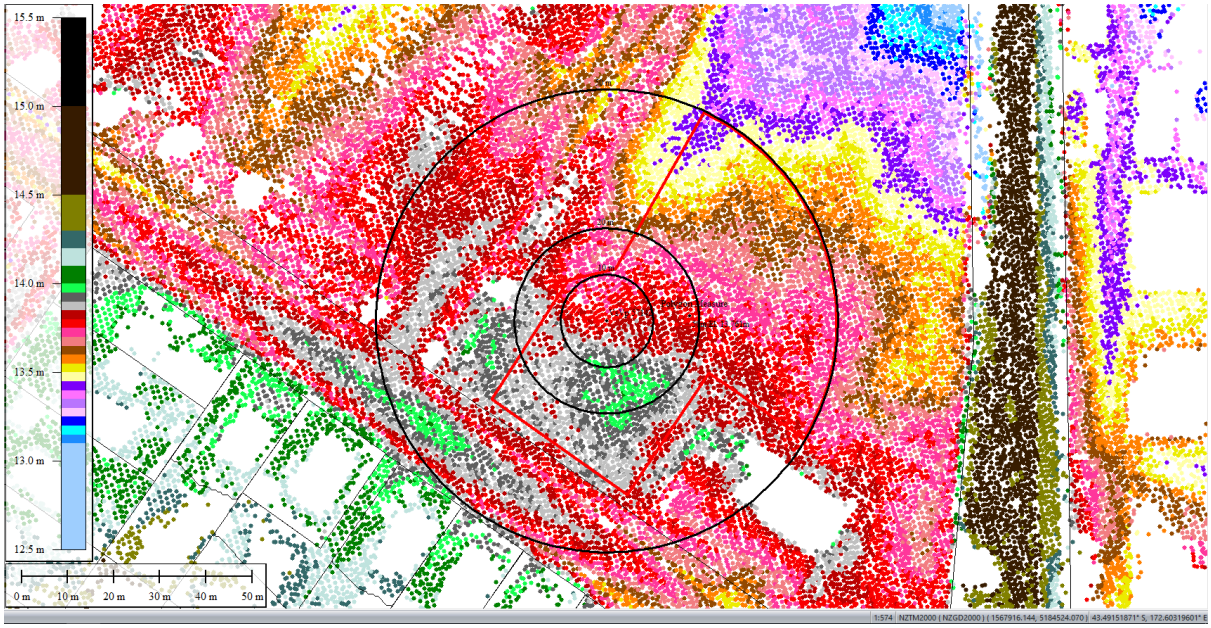

Figure 39: Ground surface elevation averaged over 50-m buffer for May 2011 LiDAR survey.

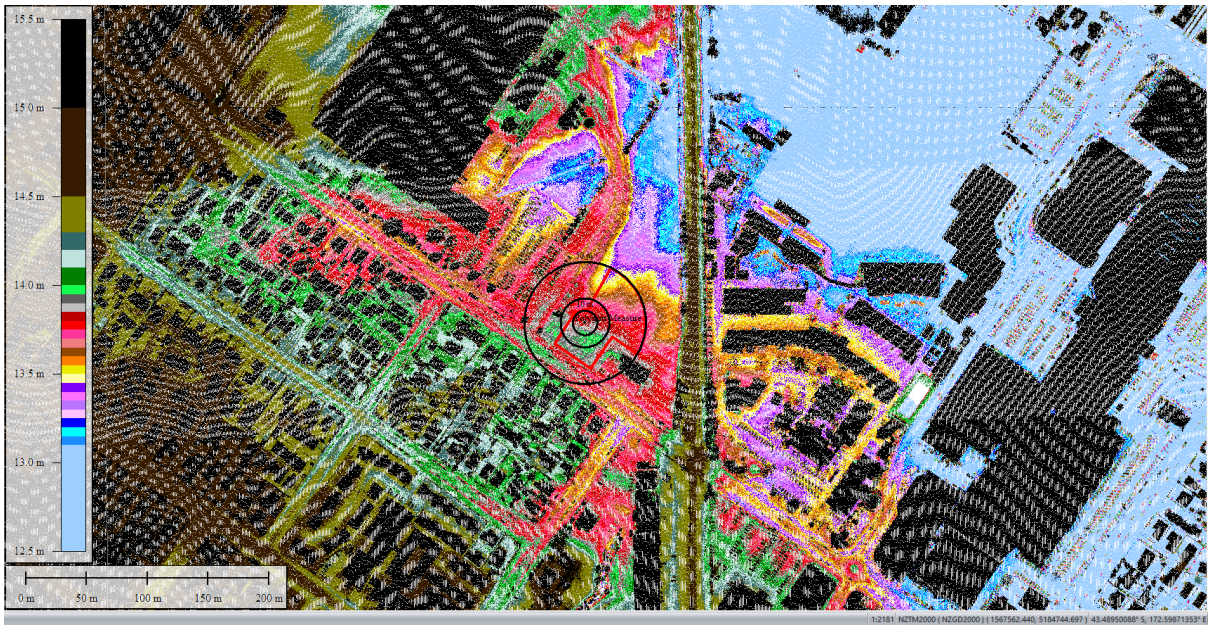

Figure 40: Sep 2011 LiDAR survey.

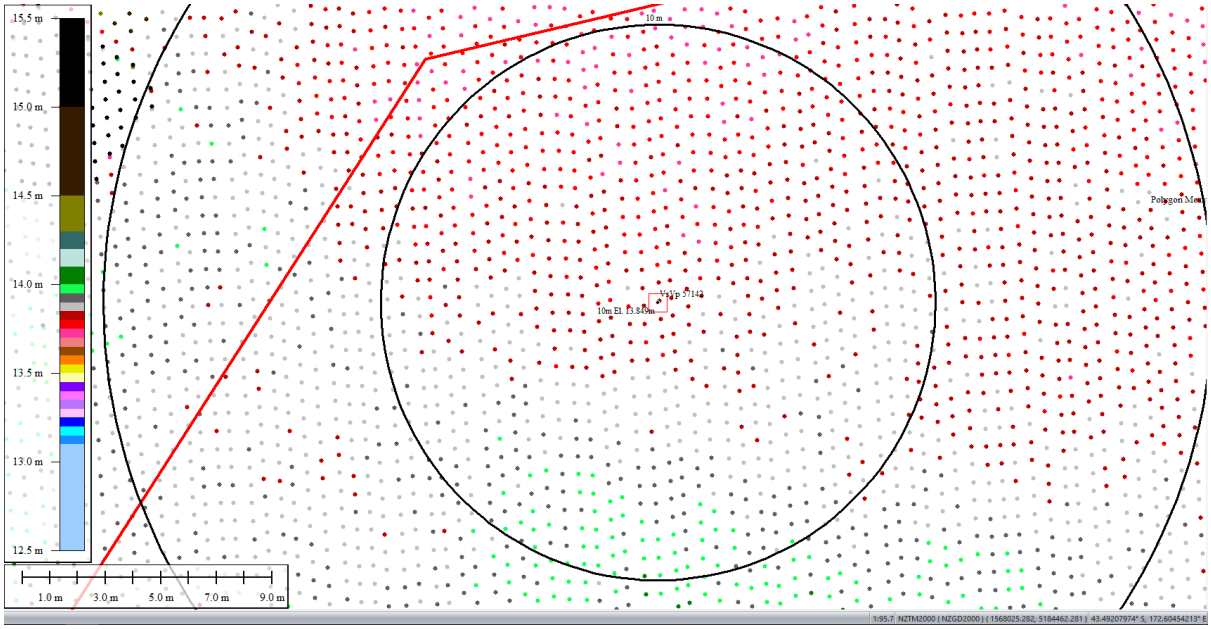

Figure 41: Ground surface elevation averaged over 10-m buffer for Sep 2011 LiDAR survey.

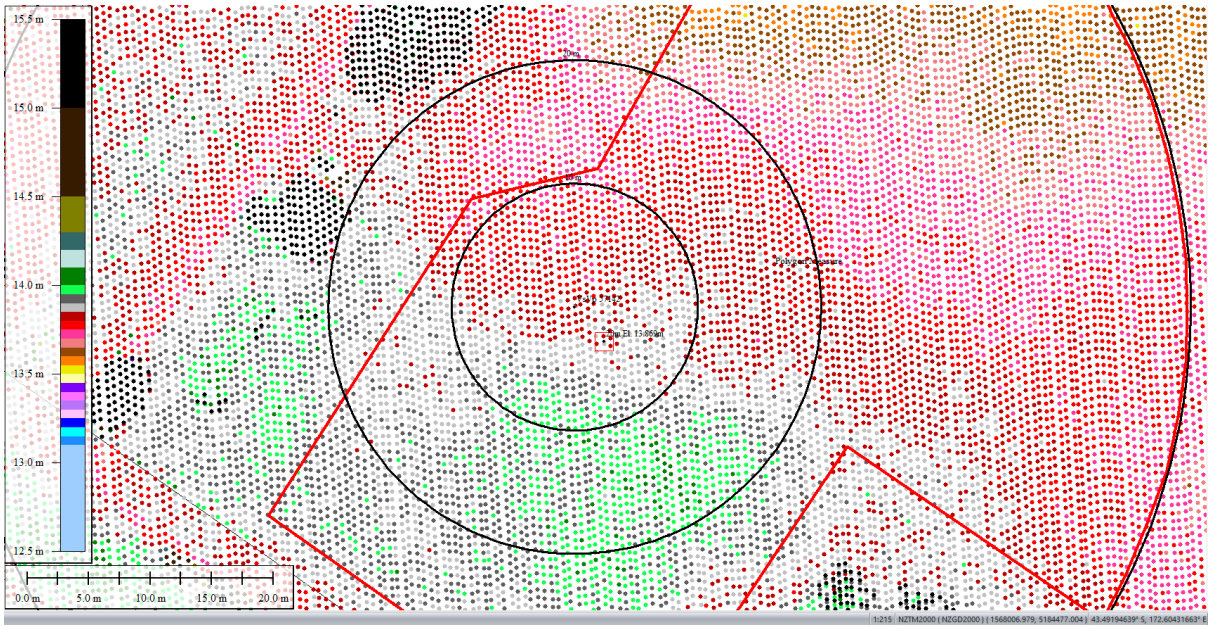

Figure 42: Ground surface elevation averaged over 20-m buffer for Sep 2011 LiDAR survey.

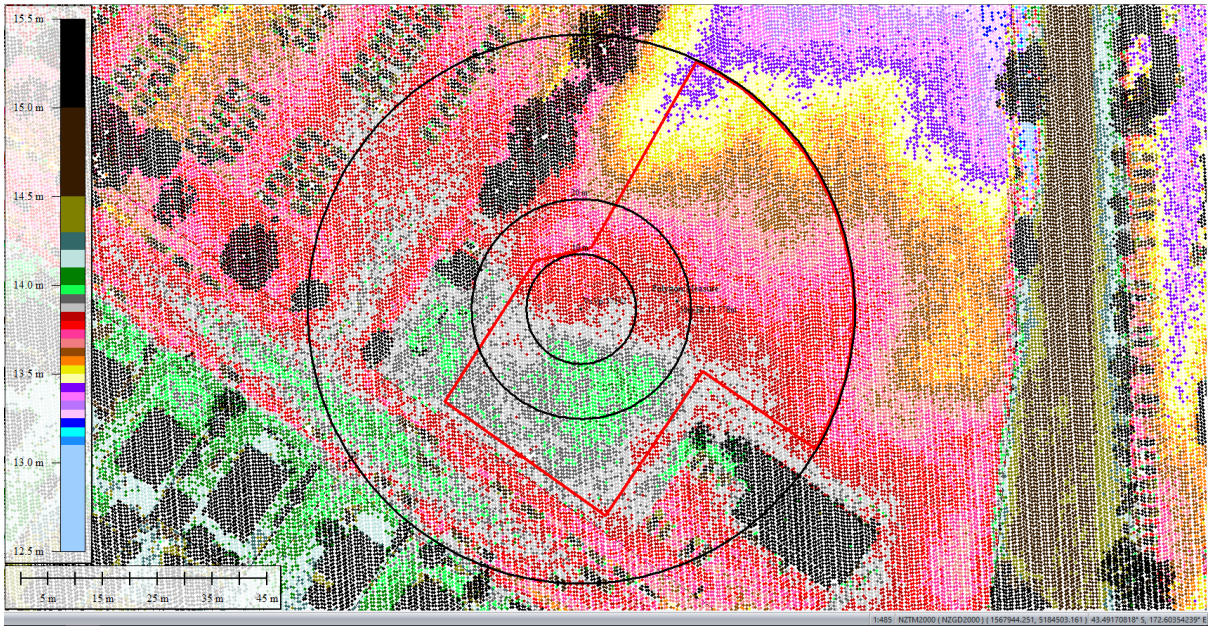

Figure 43: Ground surface elevation averaged over 50-m buffer for Sep 2011 LiDAR survey.

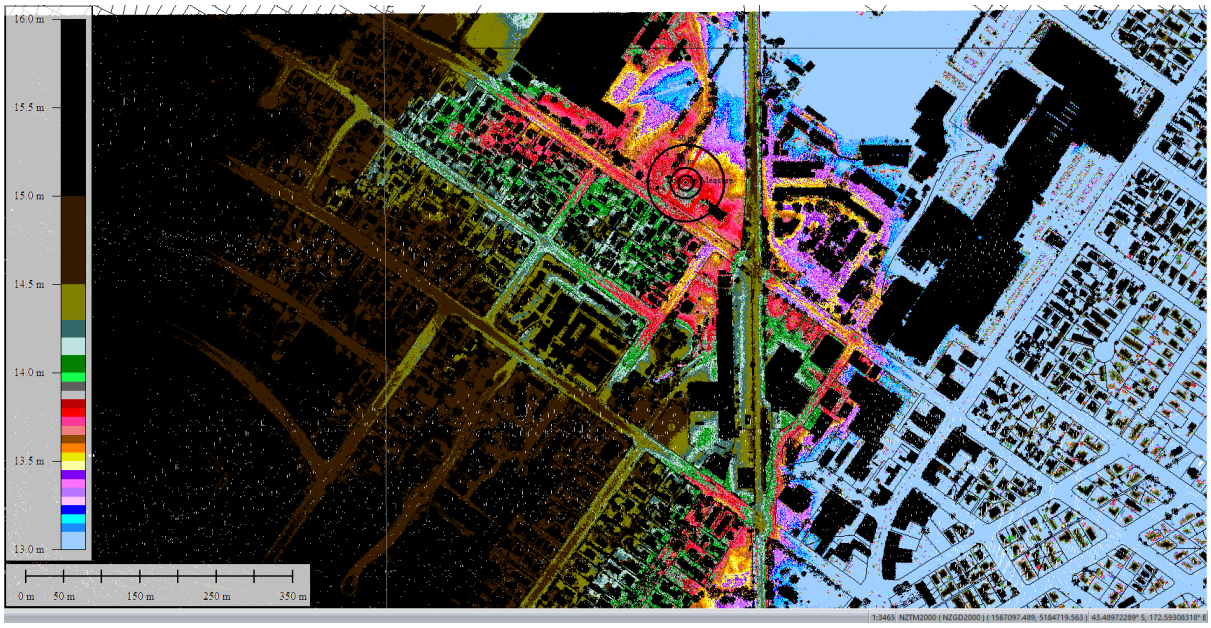

Figure 44: Feb 2012 LiDAR survey.

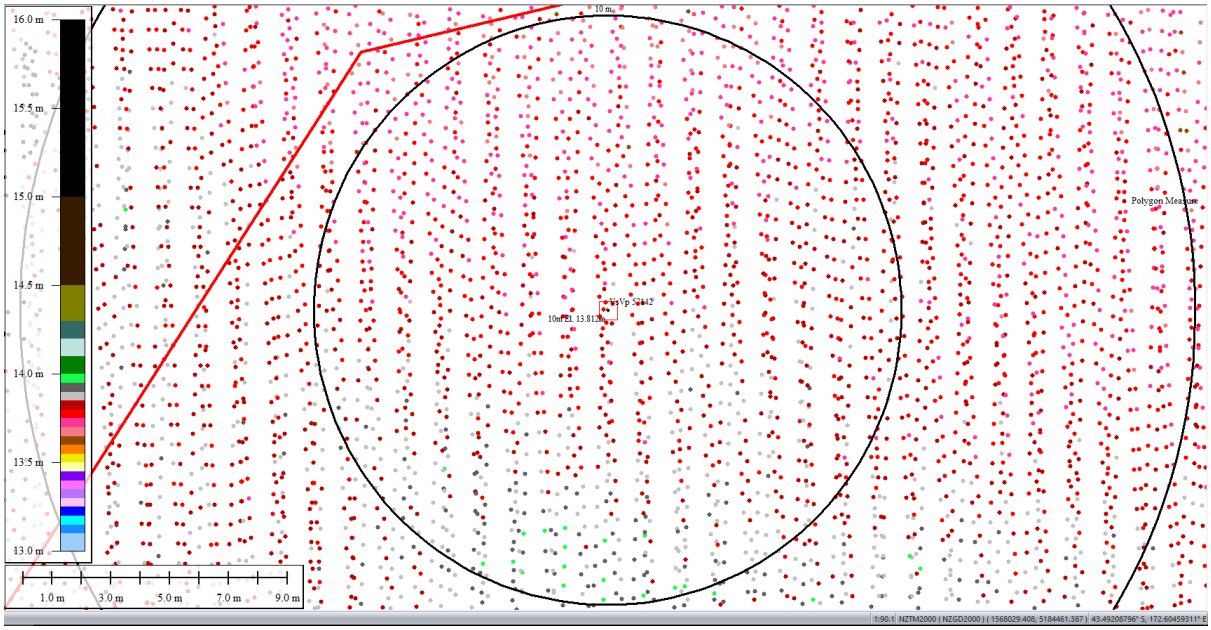

Figure 45: Ground surface elevation averaged over 10-m buffer for Feb 2012 LiDAR survey.

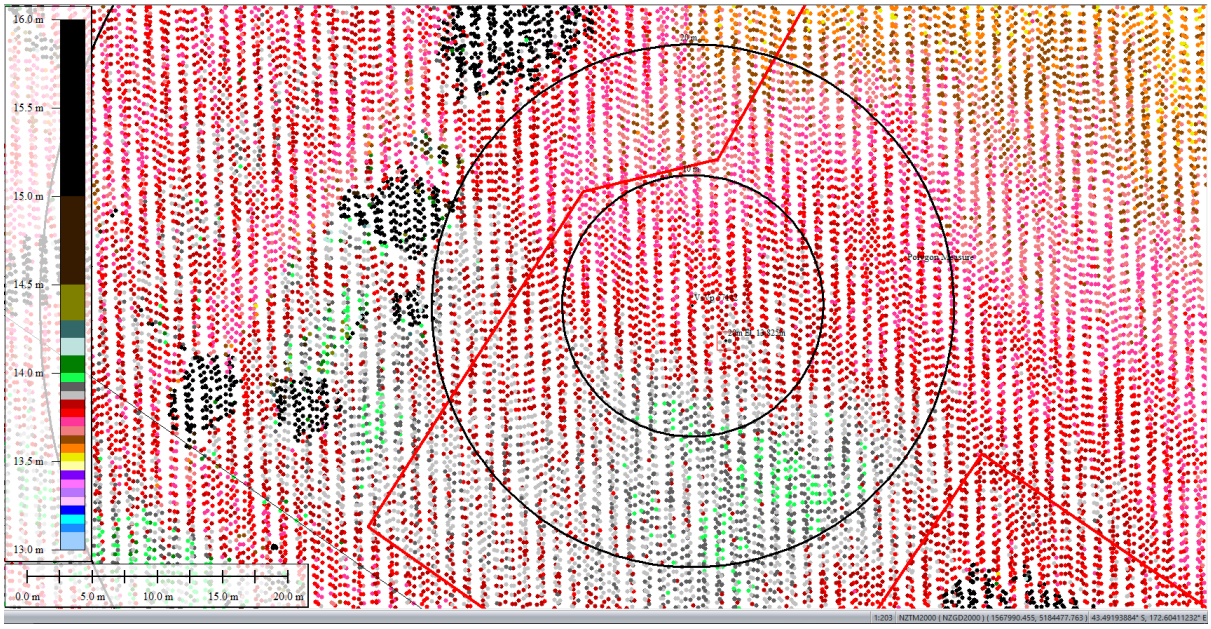

Figure 46: Ground surface elevation averaged over 20-m buffer for Feb 2012 LiDAR survey.

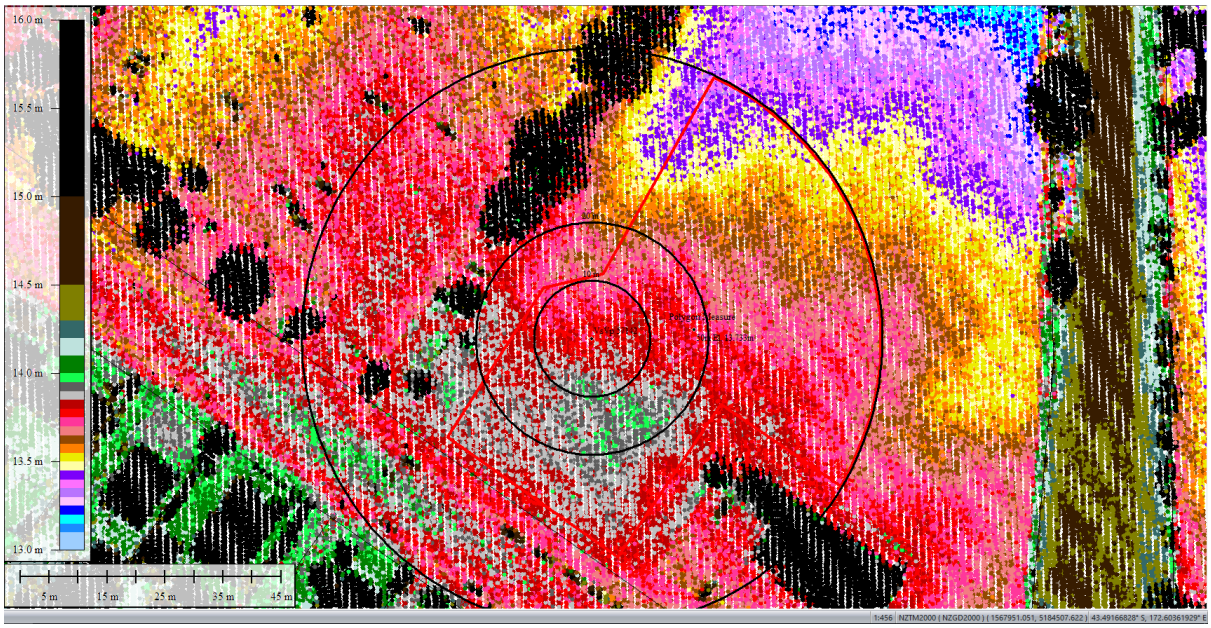

Figure 47: Ground surface elevation averaged over 50-m buffer for Feb 2012 LiDAR survey.

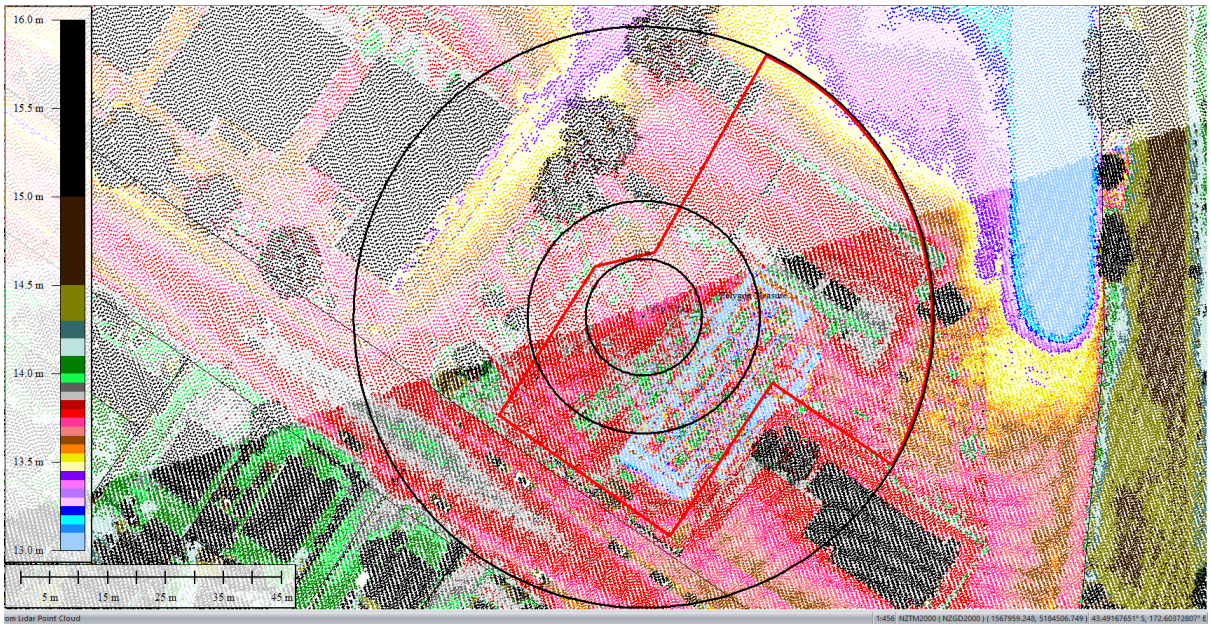

Figure 48: Oct 2015 LiDAR survey (note the change in ground surface elevation due to construction).

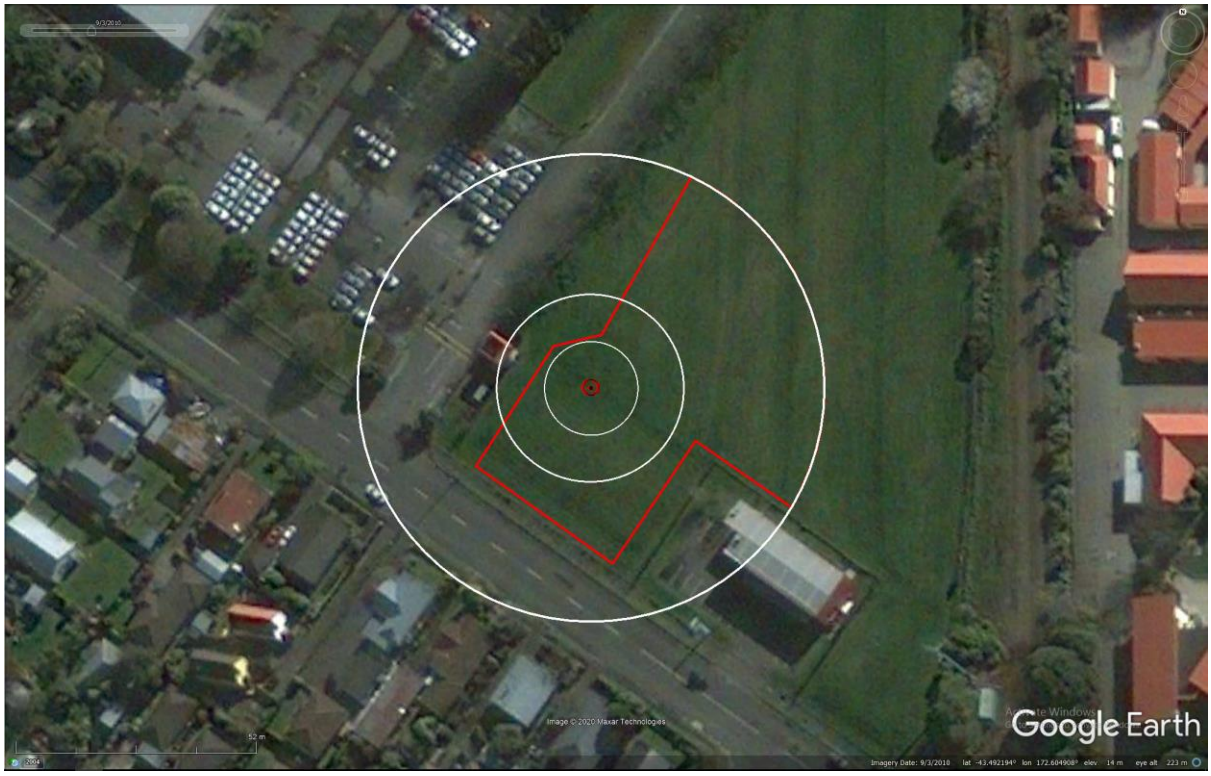

Figure 49: Absence of ejecta for Sep-10 EQ; evidence No. 1 – satellite image.

Figure 50: Absence of ejecta for Sep-10 EQ; evidence No. 2 – satellite image.

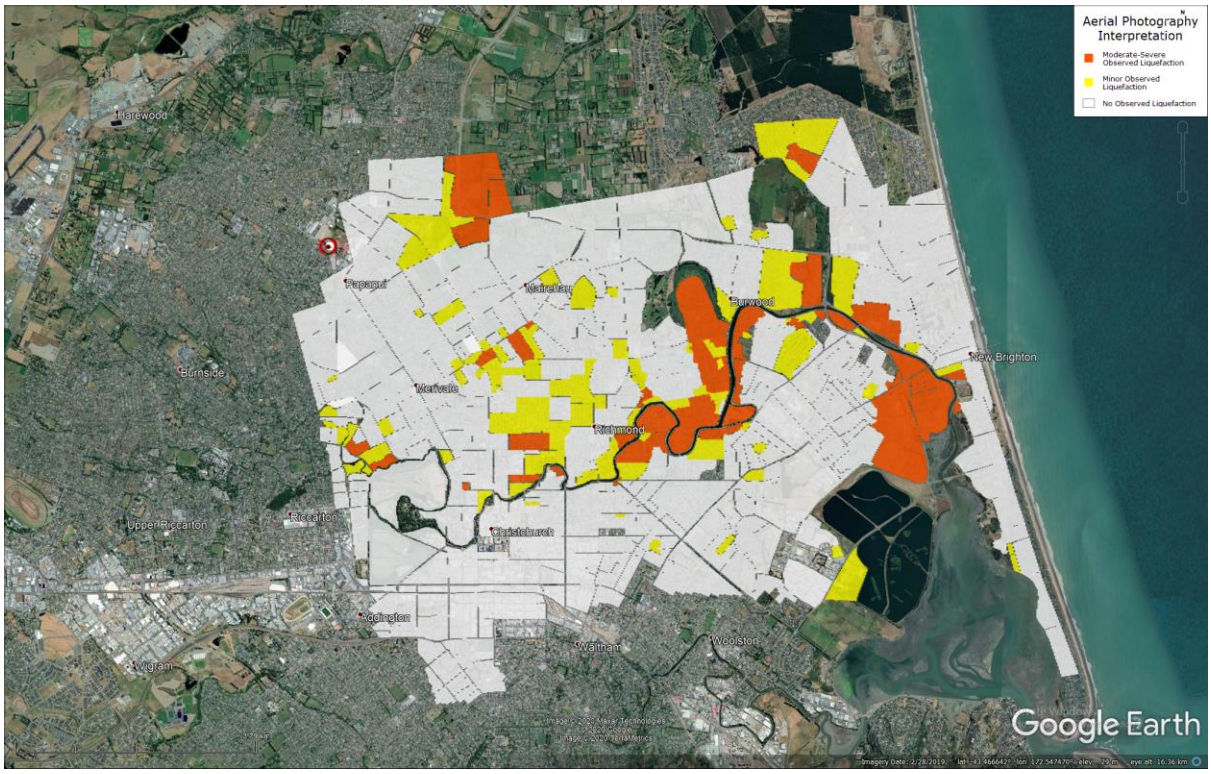

Figure 51: Liquefaction interpreted from aerial photograph for Sep-10 EQ.

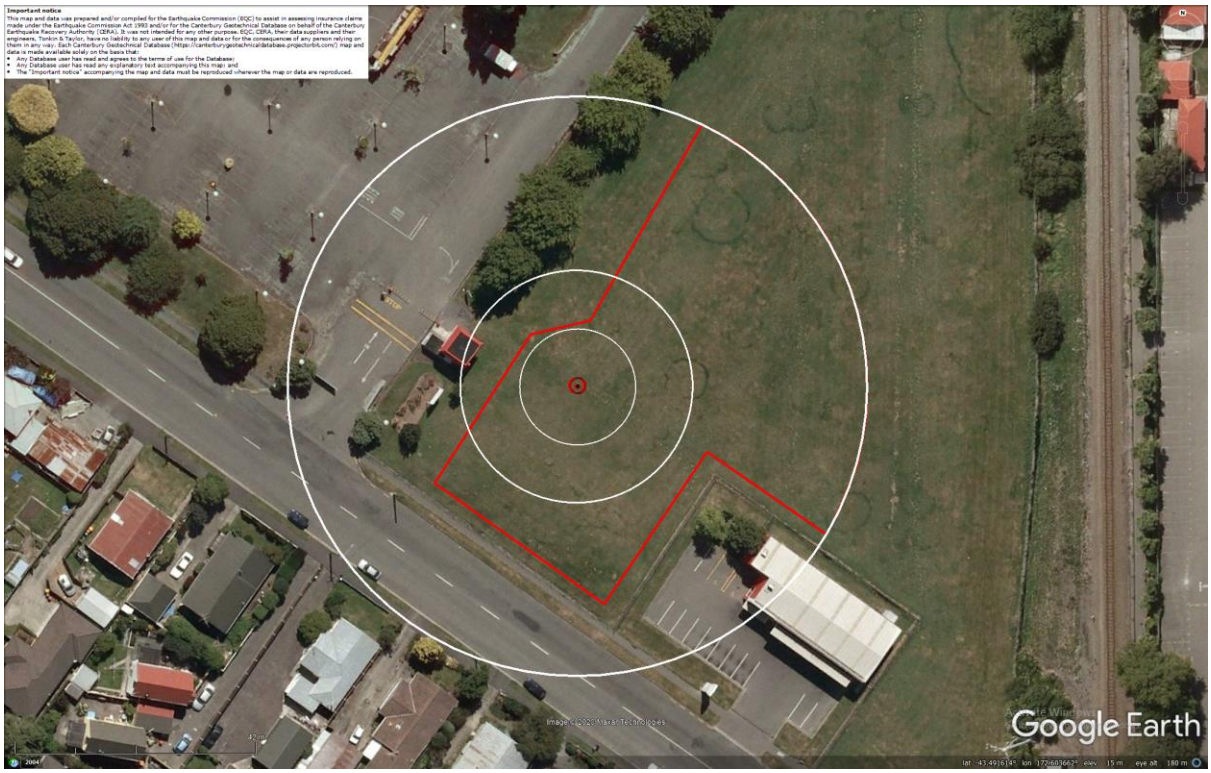

Figure 52: Absence of ejecta for Feb-11 EQ.

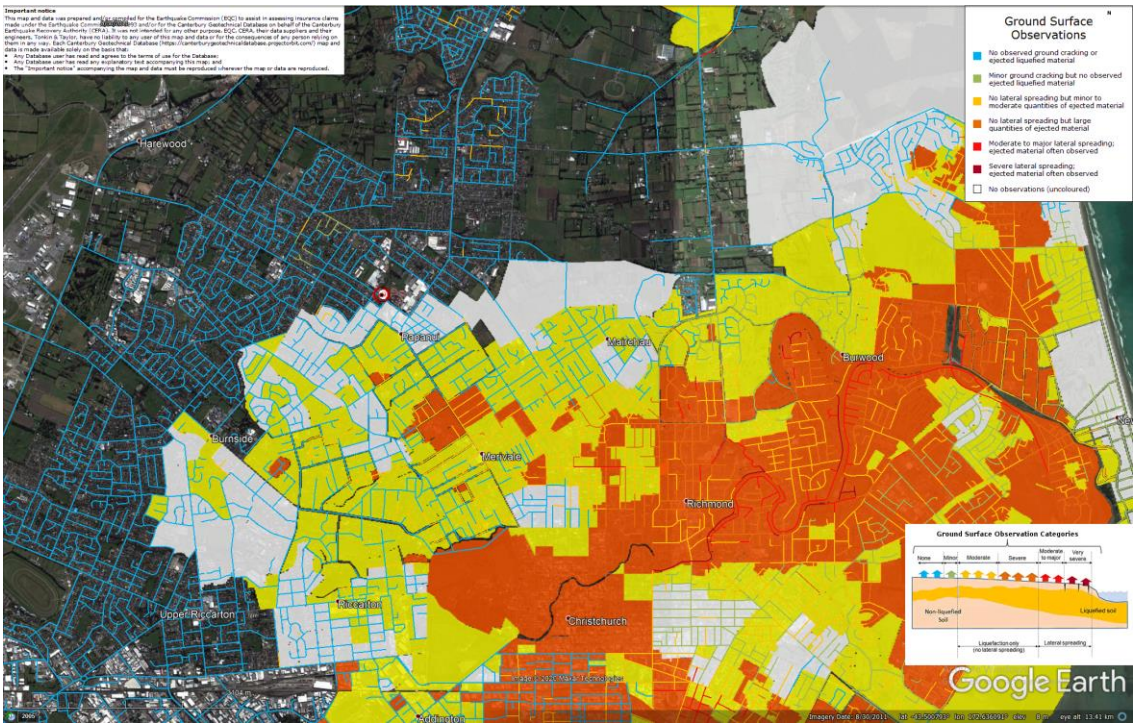

Figure 53: Liquefaction interpretation from aerial photograph and observations made by inspection teams for Jun-11 EQ.

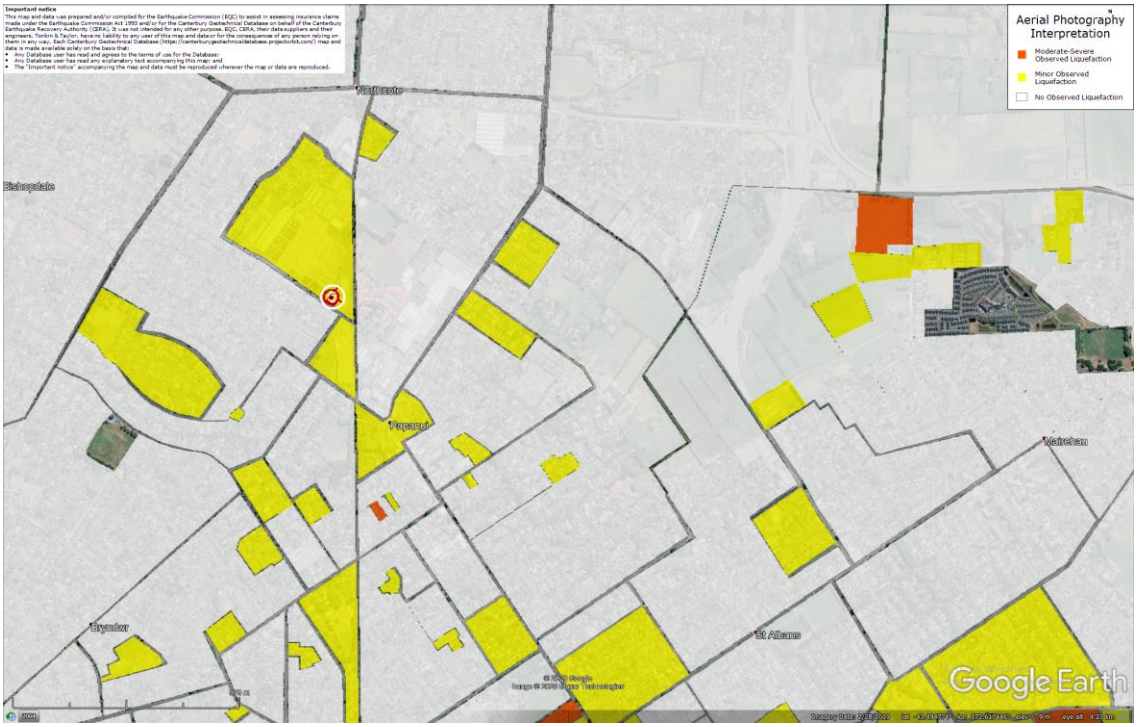

Figure 54: Liquefaction interpretation from aerial photograph for Dec-11 EQ but lack of evidence (e.g., EQC report, aerial and/or ground images) to support minor liquefaction at the site.

Figure 55: CPT locations.

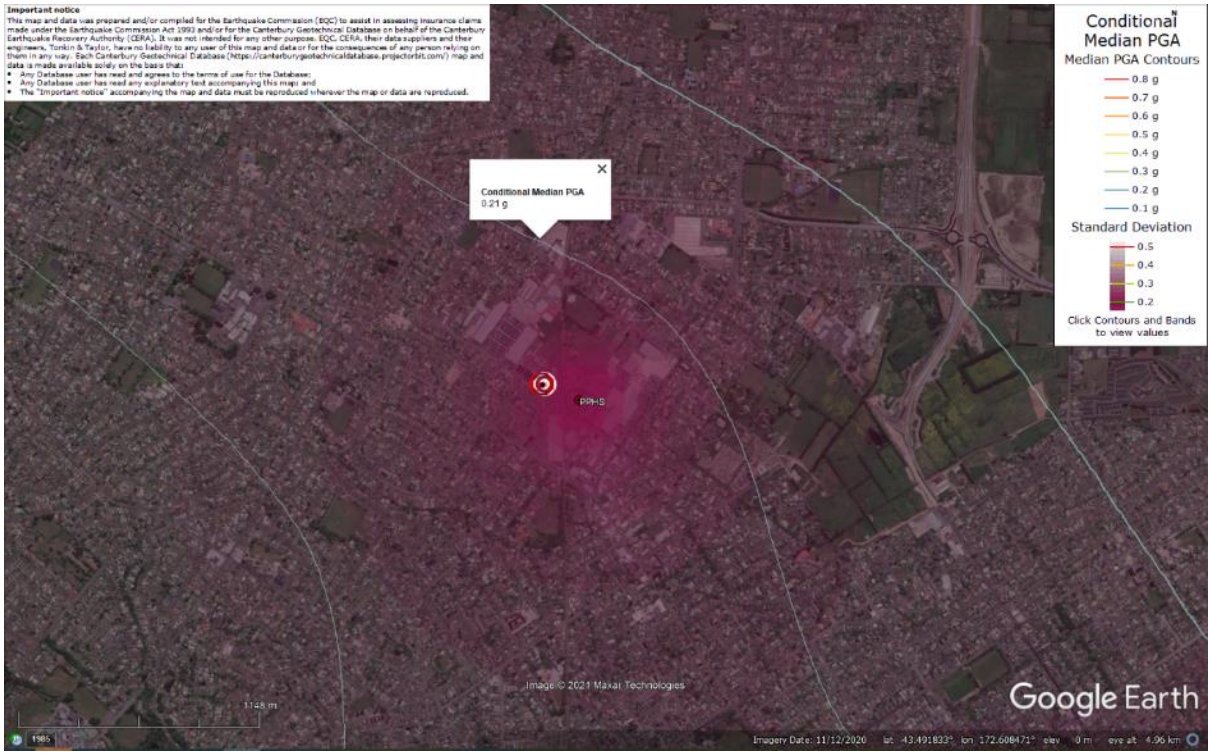

Figure 56: PGA for Sep-10 EQ (st. dev. = 0.175-0.200 ln units).

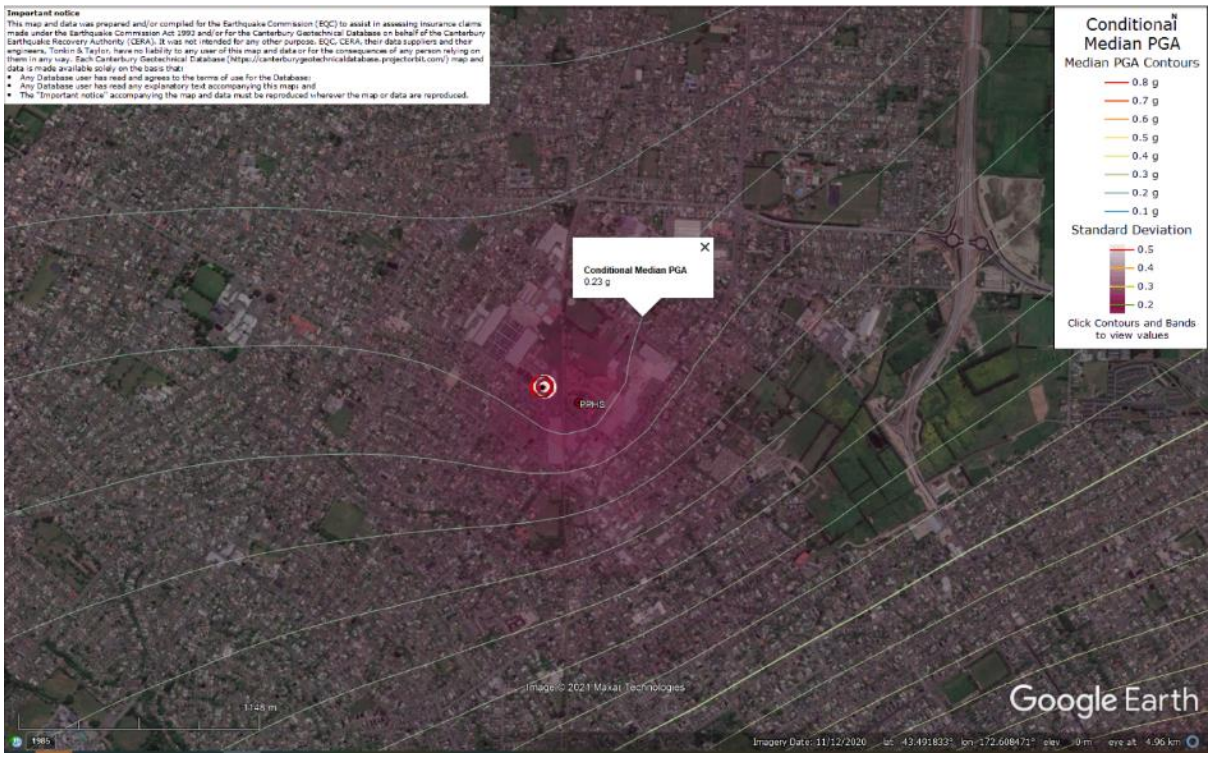

Figure 57: PGA for Feb-11 EQ (st. dev. = 0.200-0.225 ln units).

Figure 58: PGA for Jun-11 EQ (st. dev. = 0.200-0.225 ln units).

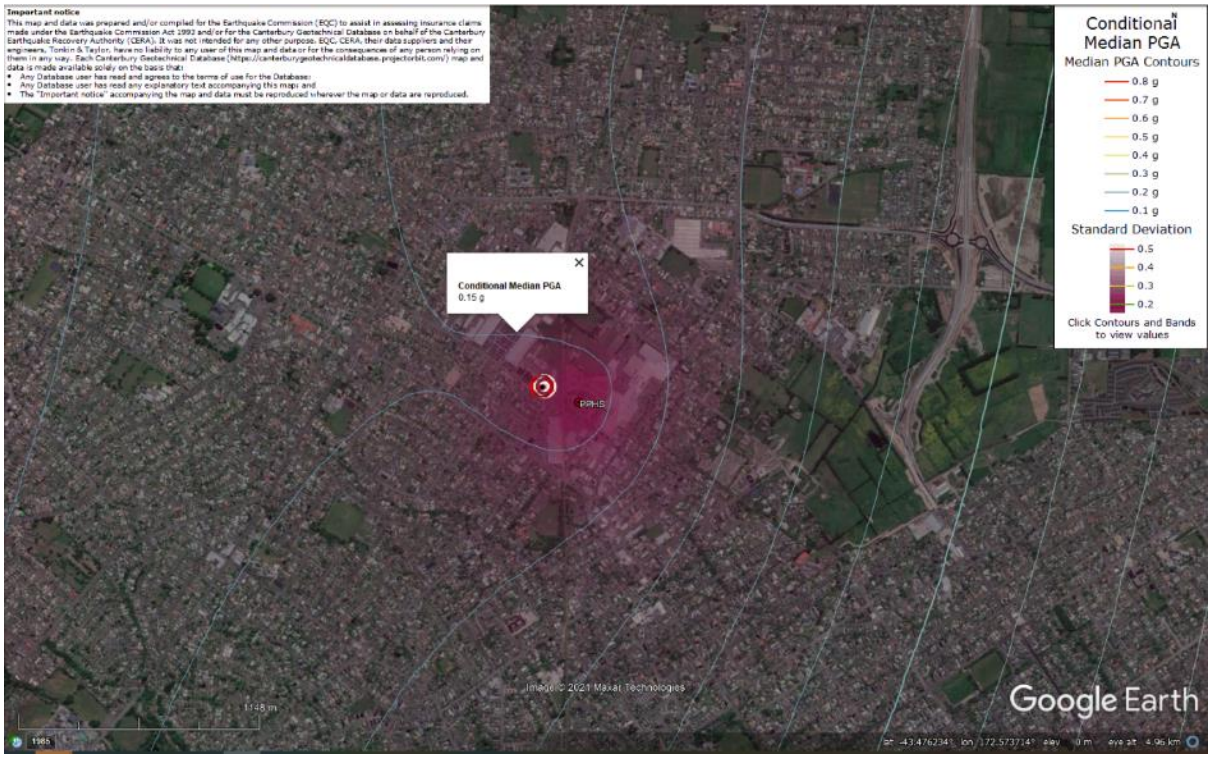

Figure 59: PGA for Dec-11 EQ (st. dev. = 0.200-0.225 ln units).

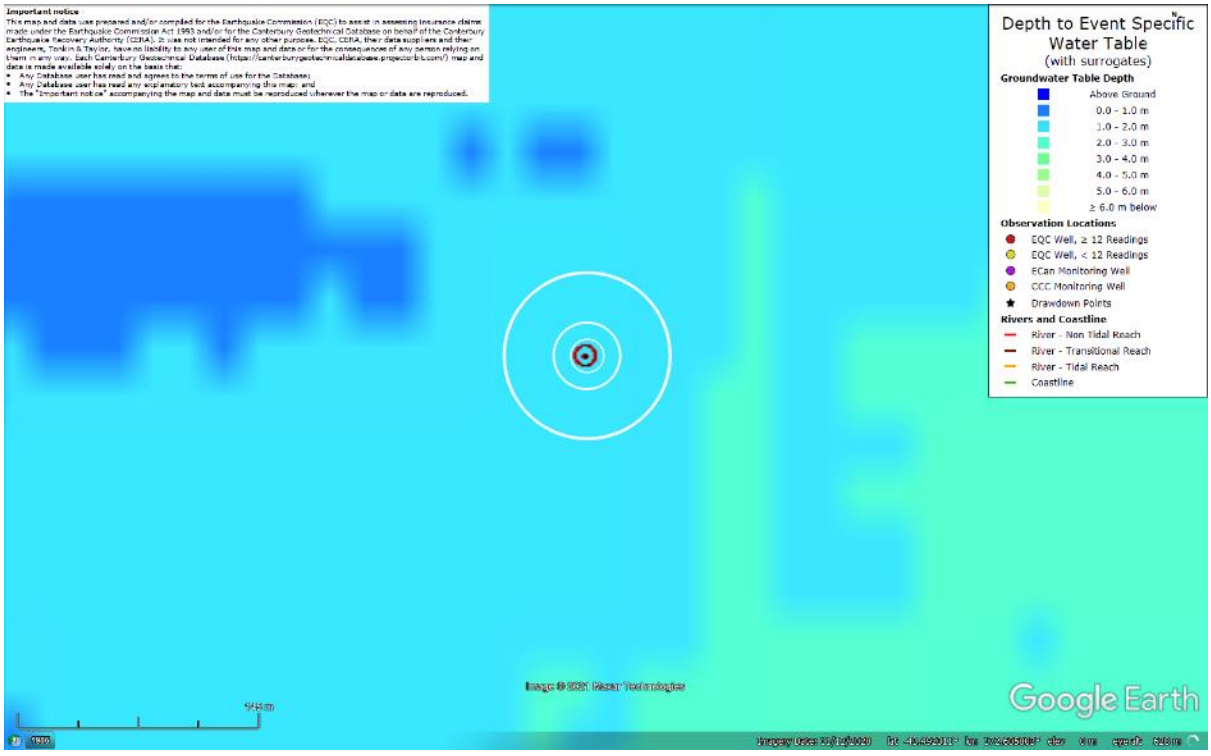

Figure 60: Depth to groundwater for Sep-10 EQ.

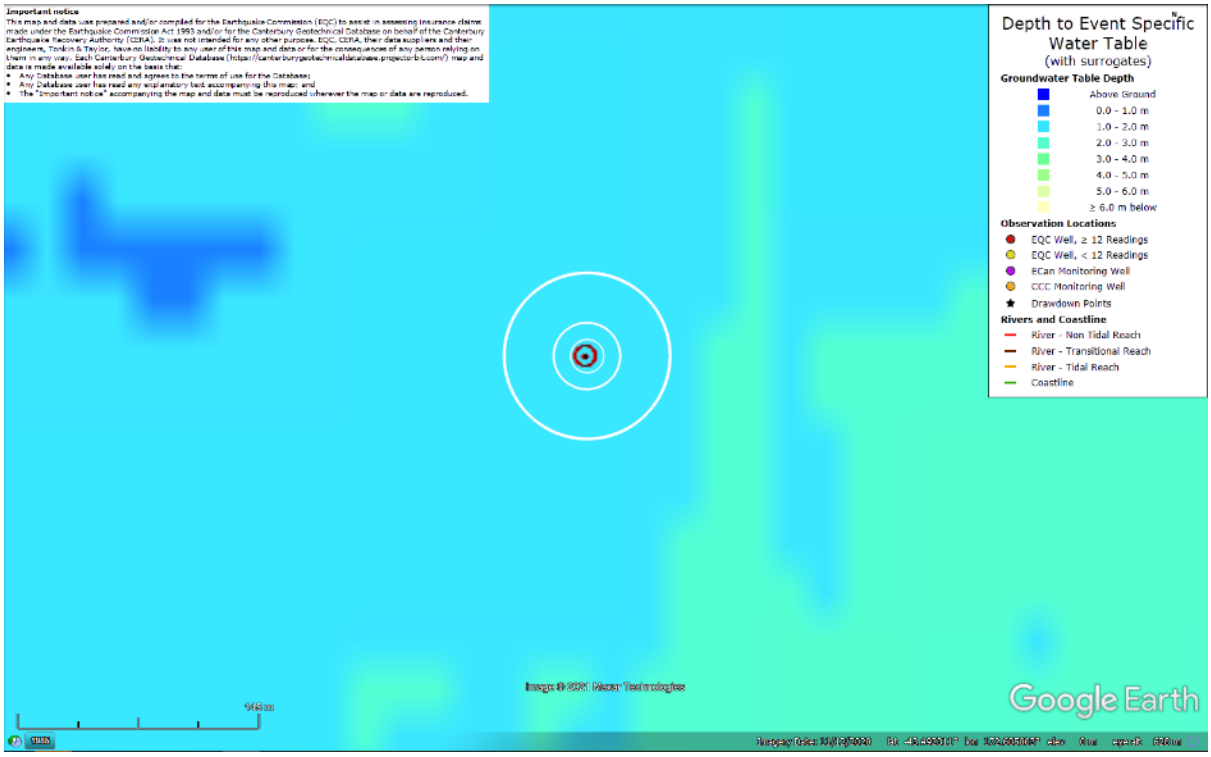

Figure 61: Depth to groundwater for Feb-11 EQ.

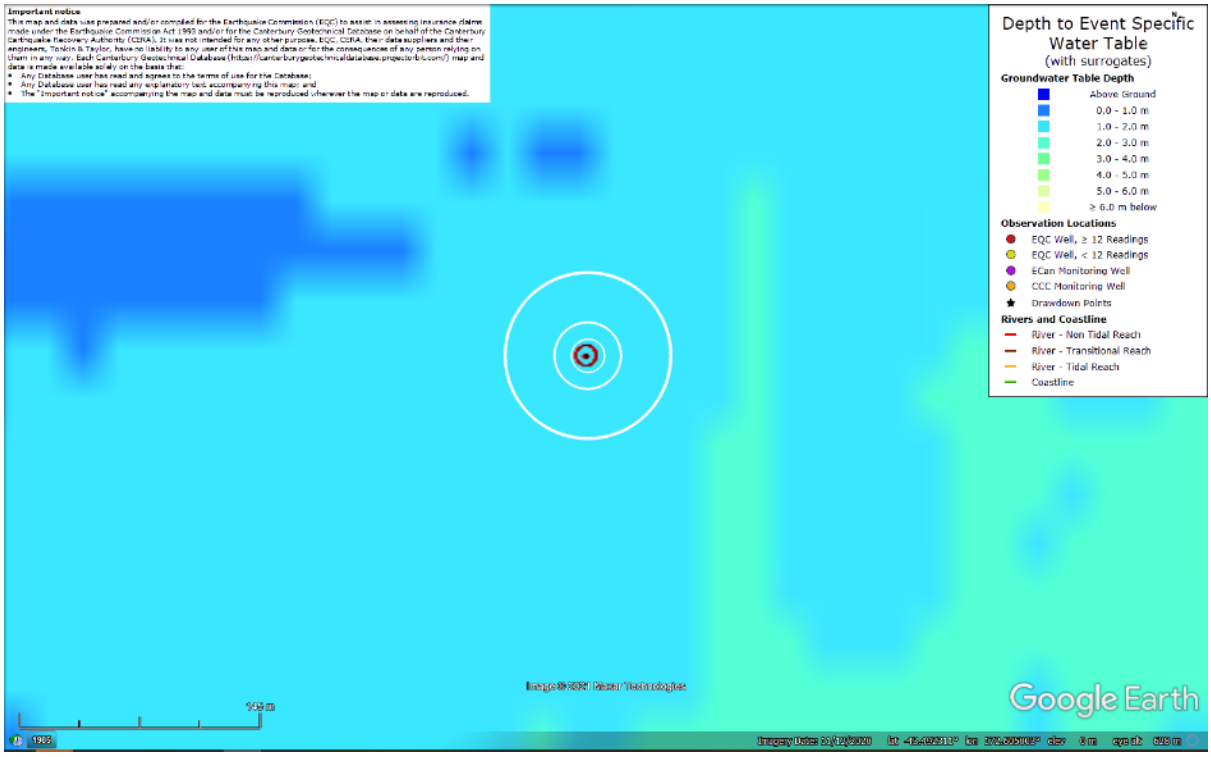

Figure 62: Depth to groundwater for Jun-11 EQ.

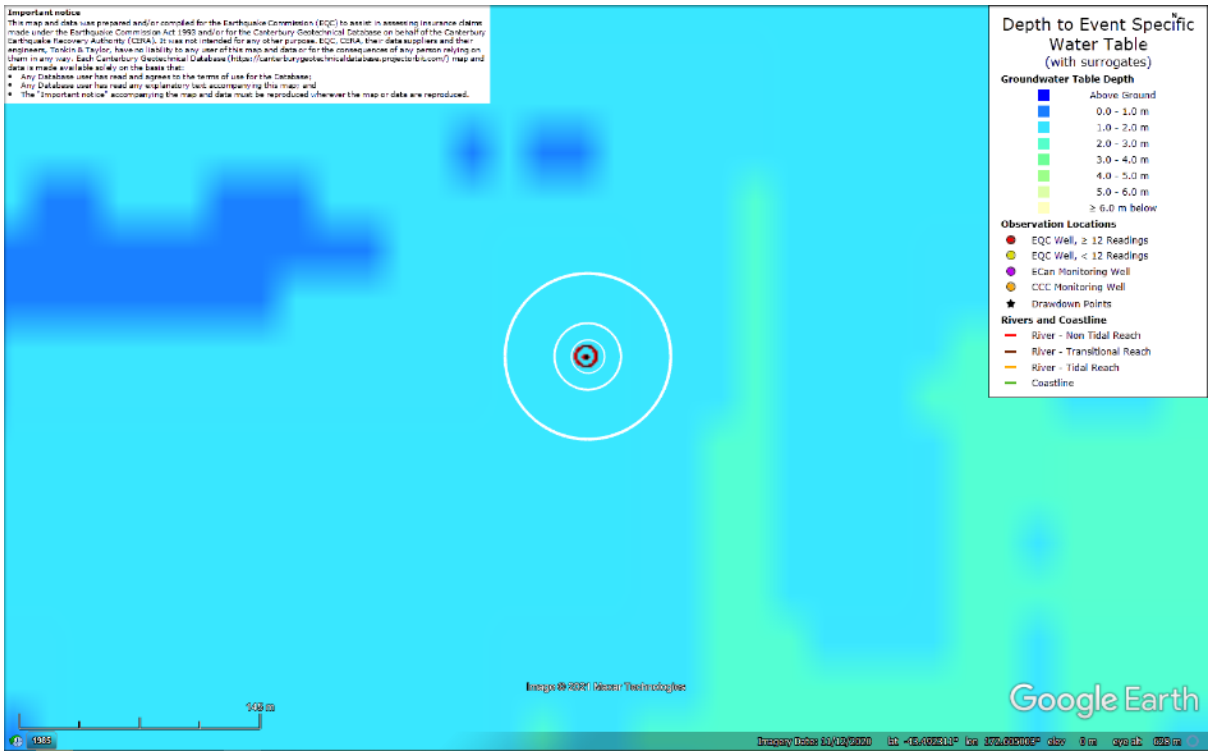

Figure 63: Depth to groundwater for Dec-11 EQ.

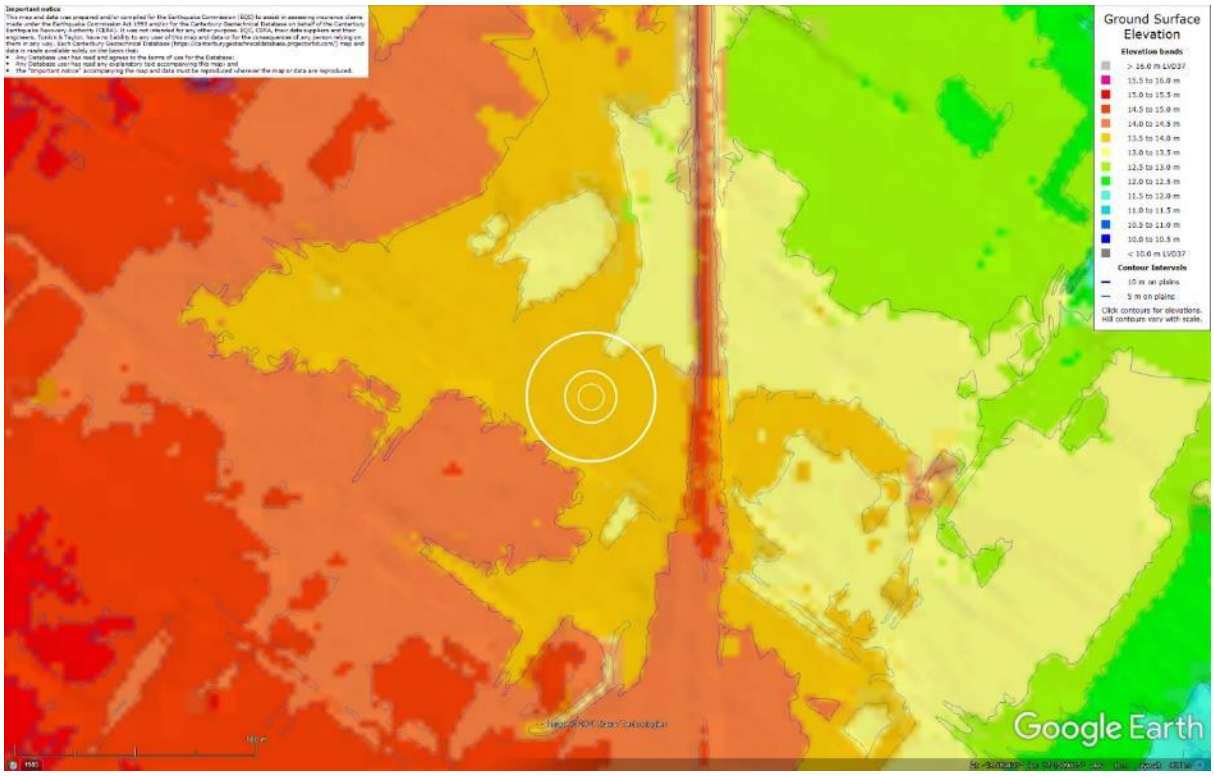

Figure 64: Ground surface elevation according to the Sep-11 LiDAR survey.

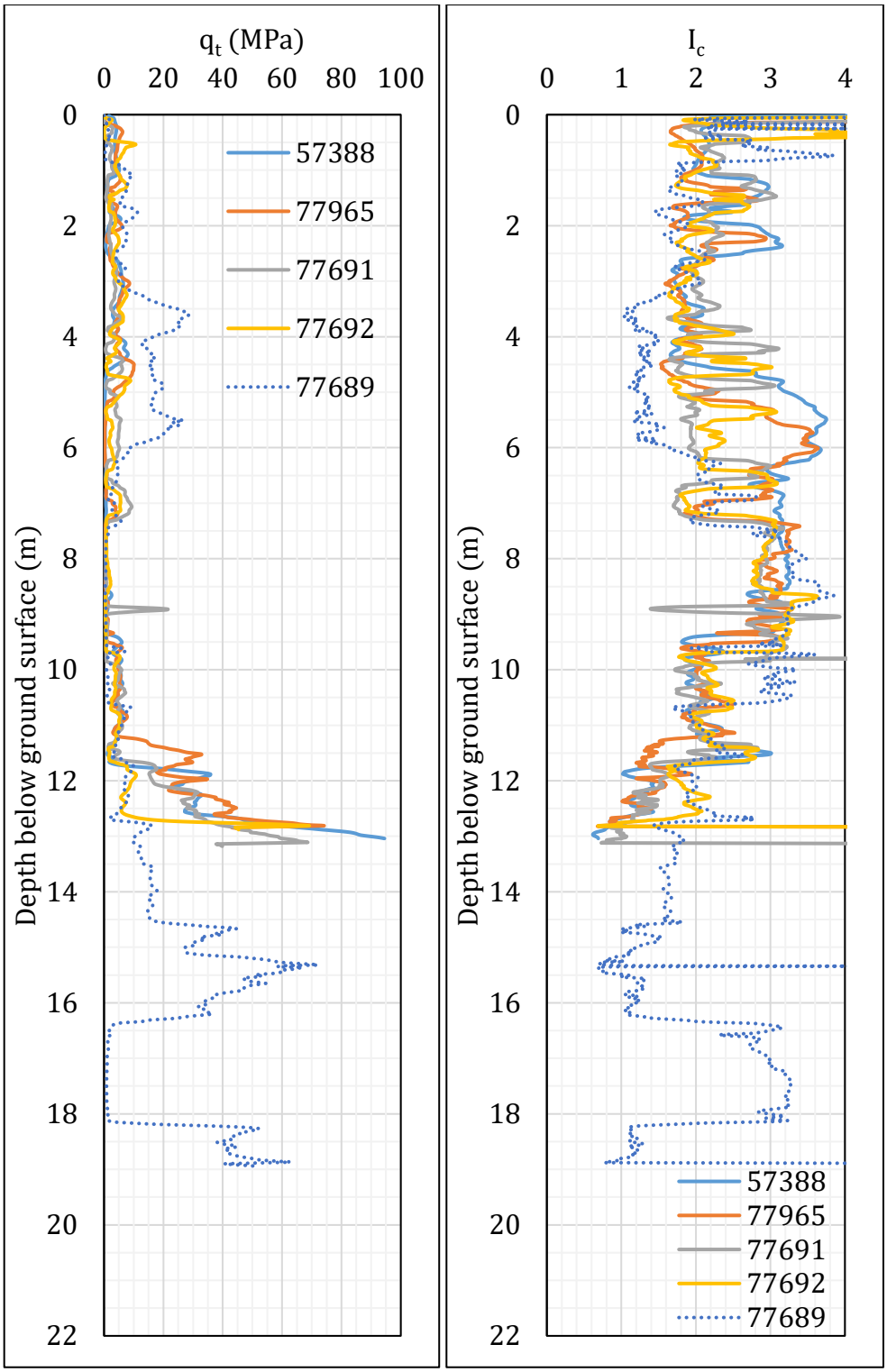

Figure 65: q_t and I_c profiles.

Note 8: The selection of CPTs for the area considered for settlement assessment (Figure 1) is based on the proximity of the CPTs to the considered areas. In accordance with that, the following table shows CPTs that were used for the volumetric settlement analysis in *Cliq v.3.0.3.2*, a CPT soil liquefaction software developed by GeoLogismiki. (The average volumetric settlements were reported in Table 8.)

Table 12: CPT profiles used in volumetric settlement analysis for areas selected for settlement assessment.

CPT ID No.	10-m buffer	20-m buffer	50-m buffer
57338 (56578)	✓	✓	✓
77965 (19274)			✓
7980*			
62756 (19258)			
77691 (19269)			✓
77692 (19270)			✓

Notes: * denotes a CPT with a penetration depth of less than 3.0 m (the reason for stopping the CPT at the shallow depth is not provided in the spreadsheet and is not obvious from the existing recordings); CPT 77689 (≈200 m away from the center of the site) was considered for volumetric settlement for a depth range from 13 m to 19 m.

Table 13: CPT-based results.

EQ Event	Parameter	CPT ID 57338	77965	77691	77692	77689	$\Delta_{13m-19m}$*
Sep-10	S_{V1D} (mm)	75	65	93	114	63	5
	LSN	12	11	17	17	7	1
	LPI	4	3	4	6	3	0
	LPI_{ish}	2	0	0	0	0	--
	$D_{FS<1}$ (m)	3.48	2.37	3.90	3.84	6.25	--
Feb-11	S_{V1D} (mm)	70	59	84	103	50	3
	LSN	11	10	15	16	6	0
	LPI	3	2	3	5	2	0
	LPI_{ish}	1	0	2	3	0	--
	$D_{FS<1}$ (m)	3.50	2.36	3.90	5.49	6.39	--
Jun-11	S_{V1D} (mm)	4	2	3	6	1	0
	LSN	0	0	1	1	0	0
	LPI	0	0	0	0	0	0
	LPI_{ish}	0	0	0	0	0	--
	$D_{FS<1}$ (m)	undet.	undet.	undet.	undet.	undet.	--
Dec-11	S_{V1D} (mm)	11	8	10	16	5	1
	LSN	1	1	1	2	1	0
	LPI	0	0	0	0	0	0
	LPI_{ish}	0	0	0	0	0	--
	$D_{FS<1}$ (m)	undet.	undet.	undet.	undet.	undet.	--

Notes: $D_{FS<1}$ = Depth to the first liquefiable layer ($FS_L<1$) that is at least 200-mm thick, as determined by the Boulanger and Idriss (2016) liquefaction-triggering procedure (P_L=50%, C_{FC}=0.13, and $I_{c,cutoff}$ =2.6), and exported from *Cliq v.3.0.3.2*; undet. = the specified soil layer was not detected; * indicates the amount of S_{V1D} and LPI to be added for a depth range between 13 m and 19 m for CPTs 57338, 77965, 77691, and 77692 due to their penetration (refusal) depths being shallower than 20 m.

Note 9: Based on the borehole log (BH 57221, Figure 55), the groundwater table is at a depth of 2.3 m below the ground surface. The soil profile consists of (1) topsoil to a depth of 0.35 m, (2) fine sand, SP, to a depth of 1.0 m, (3) silt, ML, to a depth of 2.3 m, (4) fine to medium sand, SP, to a depth of 6.55 m, (5) silt, ML, to a depth of 12.35 m, (6) sandy fine to coarse gravel, GW, to a depth of 15.0 m, and (7) fine to medium sand, SP, to a depth of 15.65 m (the end of the borehole). All SP, ML, and GW layers are the Yaldhurst members of the Springston formation. The nearby borehole (BH 62436, Figure 55) suggests that an ML layer of the Christchurch formation follows to a depth of roughly 19 m and is succeeded by Riccarton gravel to a depth of 21.75 m (the end of the borehole).